ESD-TR-71-325

ESD ACCESSION LIST
TRI Call No.
Copy No. of cys.

TRI FILE COPY

Semiannual Technical Summary

ESD RECORD COPY
RETURN TO
SCIENTIFIC & TECHNICAL INFORMATION DIVISION
(TRI), Building 1210

Seismic Discrimination

31 December 1971

Prepared for the Advanced Research Projects Agency
under Electronic Systems Division Contract F19628-70-C-0230 by

Lincoln Laboratory

MASSACHUSETTS INSTITUTE OF TECHNOLOGY

Lexington, Massachusetts

AD0737092

Approved for public release; distribution unlimited.

MASSACHUSETTS INSTITUTE OF TECHNOLOGY
LINCOLN LABORATORY

SEISMIC DISCRIMINATION

SEMIANNUAL TECHNICAL SUMMARY REPORT TO THE ADVANCED RESEARCH PROJECTS AGENCY

1 JULY – 31 DECEMBER 1971

ISSUED 26 JANUARY 1972

Approved for public release; distribution unlimited.

LEXINGTON U.S. AIR FORCE–7 FEBRUARY 1972 (37360)/265 MASSACHUSETTS

The work reported in this document was performed at Lincoln Laboratory, a center for research operated by Massachusetts Institute of Technology. This research is a part of Project Vela Uniform, which is sponsored by the Advanced Research Projects Agency of the Department of Defense under Air Force Contract F19628-70-C-0230 (ARPA Order 512).

This report may be reproduced to satisfy needs of U.S. Government agencies.

Non-Lincoln Recipients

PLEASE DO NOT RETURN

Permission is given to destroy this document when it is no longer needed.

ABSTRACT

New short-period data on source functions both of explosions and earthquakes are reported. Studies of wave propagation in inhomogeneous regions of the earth are described. First results from NORSAR are presented. Long-period noise and signal observations have been made, and some idea of NORSAR's discriminative capability is emerging. Network approaches to discrimination are being expanded. Major improvements in P-wave detection capability are in sight, with joint array and network analysis. New programs are being applied to the rapid acquisition of library information on seismic events. An increasing use of LASA for other geophysics projects is apparent.

Accepted for the Air Force
Joseph R. Waterman, Lt. Col., USAF
Chief, Lincoln Laboratory Project Office

CONTENTS

SUMMARY

This is the sixteenth Semiannual Technical Summary of the Seismic Discrimination Group of Lincoln Laboratory. Our work is directed toward acquiring as extensive an understanding as possible of seismic techniques for detecting, locating and identifying earthquakes and underground explosions, with a view to providing technical background necessary to any discussions on a treaty banning nuclear weapons tests. To the present, our work has been predominantly centered on the most effective use of LASA, the large aperture seismic array in Montana. Our interests are now broadening into the use of two recently completed arrays, NORSAR and ALPA, the World-Wide Standard Seismographic Network, and new long-period instruments. We continue to pursue research on the phenomenology of the seismic source and on several features of wave propagation. An increasing amount of pure geophysics is done with LASA, and a portion of this is described in Sec. VII of this report.

LASA and NORSAR have both been used to study explosions in order to try and improve our understanding of teleseismic aspects of the explosive source. P-waves at NORSAR from Nevadan explosions for a wide range of yields and burial depths have been studied in order to attempt to isolate effects arising from the primary pulse, the surface reflection (pP), and the spalling or slap-down that occurs shortly afterward. Very clear contributions from each of these phenomena can be isolated. This study is corroborated by studies of core phases from Cannikin and Milrow in the Aleutians from which similar conclusions emerge. It has further been possible to begin making estimates of an earthquake's size using short-period data. Core phases have been used to obtain an unencumbered view of the source, and remarkably short durations for earthquakes are measured. These convert into sizes for events of less than 10 km even up to m_b 6.0.

In recent years, large computers have allowed new approaches to problems in wave propagation. One such approximate technique has been developed which handles inhomogeneous regions at a relatively low expenditure of computing time. We report a study done on this technique to establish its usefulness in comparison with an exact method. From this work, some insight is gained into the extent of inhomogeneity necessary before approximate techniques lose their value. It is now widely accepted that many regions of the Upper Mantle contain presently active or fossil slabs. As a continuing study of the effect these inhomogeneities have on seismic propagation, we report on the effect that slabs have on the spectral content of body-wave signals. The result is difficulty in distinguishing slab effects from anelastic attenuation.

Noise studies are under way for NORSAR and ALPA. Long-period noise at NORSAR has the expected constituent coming from the Atlantic Ocean, but also a significant component appears to originate to the east of NORSAR. Such noise, which is in the same sector as Eurasia, may need some careful attention in discriminating small events. Joint ALPA/LASA noise studies have revealed sources of ocean-generated microseisms which are close to regions of low pressure as reported on weather maps. Long-period signals at NORSAR are being collected for the purpose of studying variations in character of the surface-wave train with event location. In addition to these variations, it has been possible to identify portions of the array which are less sensitive to the important shorter-period continental phase. First array-processing results are given for NORSAR discrimination purposes. Beamforming and matched-filter techniques appear to be working well, and it should soon be possible to establish a surface-wave threshold

for NORSAR; this figure will probably be seasonally dependent. LASA corrections for core phase arrivals at individual subarrays are now included in our standard Lincoln-based programs, and are proving valuable in improved processing capabilities.

With the availability of NORSAR and ALPA data, it is desirable to consider these arrays not only in isolation but in terms of a continent-wide network for discrimination. For this purpose, two new projects have been initiated. A search is being carried out to identify the most efficient means of creating a bulletin using arrays as well as single stations. Thus far, use of the LASA detection log in conjunction with a small number of WWSSN stations is proving a powerful means of obtaining a much larger earthquake catalogue. Capabilities of the long-period constituent of the WWSSN for discrimination are being assessed with a view to studying the larger population we expect to have available shortly.

Recently, we have been receiving data from the Block-Moore seismometer installed near San Diego. We report on noise and signal analysis and conclude that the best signal-to-noise ratio at this site is in the 0.03- to 0.05-Hz band. It has also been possible to generate imitation WWSSN records from these data in order to obtain an understanding of the degradation that too broad a filter has on the detectability level of surface waves. The relation between nonpropagating seismic noise and microbarograph output has been studied at LASA. We concluded that correlation techniques enable nonpropagating noise to be significantly reduced.

The large amount of data now available in our Lincoln facility is being documented for access by a program called LISTAR. This program, based on the remote-console accessed Lincoln 360, should enable us to generate lists of events of interest within minutes, and have full information on how to find relevant data. The Analysis Console has been the subject of a movie designed to demonstrate its capabilities; it also stars in a BBC television production on solid earth geophysics.

Finally, LASA has been used to demonstrate for the first time the presence of seismic phase PKJKP, and hence the rigidity of the inner core. This issue has been in doubt for 35 years, but it now seems possible to assign a shear velocity of 2.95 ± 0.1 km/sec to the inner core. Furthermore, LASA is being used to study fine structure on the boundary of the inner core.

D. Davies

GLOSSARY

ALPA	Alaskan Long-Period Array
IGPP	Institute of Geophysics and Planetary Physics, University of California, La Jolla
LASA	Large Aperture Seismic Array
LP	Long Period
LPE	Long-Period Experiment
NORSAR	Norwegian Seismic Array
NOS	National Ocean Survey
SAAC	Seismic Array Analysis Center
SATS	Semiannual Technical Summary
WWSSN	World-Wide Standard Seismographic Network

SEISMIC DISCRIMINATION

I. THE SEISMIC SOURCE

A. OBSERVATIONS OF pP IN THE SHORT-PERIOD SOURCE FUNCTION OF NTS EXPLOSIONS RECORDED AT NORSAR

At teleseismie distances, the effeetive source function of explosions contains not only the primary P-phase, but also the pP-phase whieh is reversed in polarity and arrives within a second after the P-pulse of most explosions. A third pulse is often seen with the same polarity as the P-pulse and later than pP. The detection of pP-phases has been done predominantly by frequency domain analyses[1-3] of the first few seconds of the P-wave, because interferenee between the P and pP makes it diffieult to time the pP onset. Implieit in sueh studies is the assumption that the pP-pulse has the same shape as the P-pulse exeept for the change of polarity. In the frequeney domain, this produees a sharp sealloping of the amplitude speetrum of the waveform, giving minima at periods $T_n \simeq \tau/n$ for $n = 1, 2, \ldots$, where τ is the delay time for pP relative to P. If, however, the pP has a different shape and a lower amplitude than the P-pulse and other phases are present, then the speetral minima may disappear or be ineonelusive,[3] as is often the ease.

An alternative approaeh to the separation of P- from pP-phases is to simply remove the time-domain instrument response from the observed data and interpret the deeonvolved reeords as displaeement souree funetions. In this manner, one obtains a direct pieture of the P, pP and other phases whieh must be ineluded in any realistie souree funetion.

This is being attempted first with explosions of known depth and loeation. Figure I-1 shows a suite of eleven NTS events reeorded at NORSAR. The shot depths indieated for these events are taken from the explosion summary by Springer and Kinnaman.[4] The waveforms are arranged in order of inereasing depth and aligned in time at the first trough, rather than at the first peak. This was done in order to eliminate the effeet of the variable rise time of the first motion, and it also eorresponds to the maximum displaeement of the impulse displaeement response of the short-period seismometer at NORSAR.

Each waveform is a steered beam at either the interim array of NORSAR, at the subarrays near Faldalen or Oyer, or at the temporary array OONW near Lillehammer. The interim array eonsists of a single seismometer from eaeh subarray of the eomplete NORSAR array.

The clearest pP-phasc oeeurs on the seismogram of Stinger at Oyer. Due to the short duration of the P-pulse, the pP is elearly separated, inverted and delayed about 0.9 sec relative to P. On the other seismograms, the pP-phases are not nearly as clear, due to both impcrfeet rcflection of P at the free surfaee and the lower frequeney content of the primary pulse. On many events there is a strong seeond trough, which has the wrong polarity and time for pP. This pulse has a time delay which inereases with depth and is part of the effective souree funetion. For example, at Oyer there is inerease in delay time of almost a seeond for this seeond trough for events Purse down through Boxear. Similarly, on the interim array, Hutch, Blenton and Shaper are quite similar, whereas Handley has a seeond trough almost a seeond later than the trough in the three shallower shots.

The seismograms of Fig. I-1 were deconvolved by removing the impulse displacement response of the short-period seismograph which is displayed to the left of Stinger and Knox. As shown, this response has been convolved with an attenuation operator with $t^* = 0.25$ to simulate most of the average earth attenuation from the NTS area to NORSAR.[5] The deconvolved displacement waveforms are shown in Fig. I-2 aligned in time at the first peak. Neglecting the effect of layering under the receiver, these seismograms can be interpreted as the effective far-field displacement source for each event. The first peak of each wave is the direct P-pulse, followed by a trough which is the pP-phase. A second peak, which is often strong, corresponds to the second trough seen on the original waveforms. It has also been noted by Kulhánek[1] on other NTS shots recorded by the Swedish seismic network.

Figure I-3 shows a plot of the delay times vs depth for pP picked directly from the deconvolved seismograms. The receiver array is indicated for each event to show that the pP delay times are not receiver-dependent. Although the times generally increase with depth, there is considerable scatter in the data. In order to isolate the source-region effects, the same data are plotted in Fig. I-4, with symbols indicating the NTS source region. These data indicate that Yucca Flat has average compressional velocities somewhat slower than Pahute Mesa.

Average compressional velocities for the media above each shot were calculated from the formula

$$\bar{\alpha} = 2h/\tau$$

where h is the shot depth in kilometers, and τ is the observed pP-P delay. The data for these calculations are listed in Table I-1. Kulhánek[1] used observed spectral minima ~1 Hz to infer pP delay times for NTS shots recorded by the Swedish seismic network. His average velocities and the velocities in Table I-1 are superposed in Fig. I-5. The events are separated into three NTS regions, namely Yucca Flat, Pahute Mesa and Hot Creek Valley. Of the two sets of data, the only common events are Boxcar and Faultless, which show good agreement between the two methods.

TABLE I-1

DELAY TIME τ VS DEPTH FOR EVENTS STUDIED AT THREE TEST SITES

NTS Region	Date	Event	Depth (m)	τ (sec)	$\bar{\alpha}^*$ (km/sec)
Pahute Mesa	5/9/69	Purse	599	0.75	1.59
	3/22/68	Stinger	668	0.85	1.57
	4/26/68	Boxcar	1158	1.10	2.10
	3/26/70	Handley	1207	1.15	2.09
Yucca Flat	7/16/69	Hutch	549	0.65	1.69
	4/30/69	Blentan	557	0.75	1.49
	3/23/70	Shaper	561	0.80	1.40
	9/6/68	Noggin	582	0.80	1.46
	2/21/68	Knox	645	0.95	1.36
	10/18/67	Lanpher	715	0.95	1.51
Hat Creek Valley	1/19/68	Faultless	975	0.90	2.16

*Average velocity of the rocks over the shot.

The data for Pahute Mesa indicate that the average velocity varies linearly from about 1.5 to 2.5 km/sec over the depth range 600 to 1400 m. Average velocities for Yucca Flat vary from about 1.1 to 1.7 km/sec from depths of 460 to 760 m, most of the data scattering about 1.5 km/sec. These velocities are reasonable when compared with a cross section of the Yucca Valley given by Springer.[6] The alluvium surface layer varies from 0.4 to 0.9 km/sec, and the underlying tuff stratum has velocities up to 1.5 km/sec.

Returning to Fig. I-3, it appears that the absence of a clear pP on the original seismograms can be explained by the shape of the pP-pulse on the deconvolved seismograms. For example, the P- and pP-pulses of Stinger appear equally sharp in this figure which accounts for their clarity on the original seismogram. However, for Boxcar and Handley, the pP-pulses on the deconvolved seismograms are considerably broader and of lower amplitude than the P-pulses. This imperfect reflection at the free surface produces the broad, indistinct pP-phases seen on the original seismograms.

Finally, we note that the second peak on the deconvolved seismograms is often large, for example on Blenton and Shaper. This pulse may be due to the spalling of the ground surface over the shot and should be included as part of the effective source function, observed at teleseismic distances. An example of spalling is shown in Fig. I-6. This shows the vertical components of acceleration and displacement observed on the ground surface over a "typical" test shot,[7] which unfortunately is not identified. The first acceleration peak is the direct wave arriving at the surface, which after reflection produces the pP-phase observed telseismically. The second peak is caused by the "slap down" of the rock material after about a second of free fall. This acts like a secondary source which then radiates out telseismically with the same polarity as the primary P-pulse.

C. W. Frasier

B. SOURCE FUNCTION FOR EXPLOSIONS FROM CORE REFLECTIONS

In the last two SATS (31 December 1970, DDC AD-718971; and 30 June 1971, DDC AD-728210), I discussed in some detail the problem of looking at source-time functions for explosions. This problem is important for understanding the physical basis for discrimination. It has been clear for some time that the teleseismic P-wave, although a clear and simple signal, often is overprinted with confusing detail of lateral heterogeneity in the mantle. The best way to look seismically at the source seems to be by means of a core reflection, for which P-waves have emerged nearly vertically and are thus least prone to see lateral variations. In earlier reports, the phase PKiKP, reflected from the inner core, has been used. The assumption was made that the inner-core boundary was sharp and, thus, that reflection from it gave as undistorted a picture of the short-period source function as seismology could provide. Recent work on Milrow and Cannikin has shown this assumption to be incorrect. As a result of new data, one can now construct both a revised source function and a tentative structure for the inner-core boundary (see Sec. VII).

Figure I-7(a-b) shows LASA signals for phases PeP, PKiKP and PKKKP from Milrow and Cannikin. PKKKP is particularly remarkable. It has a $dT/d\Delta$ of 2.3 sec/deg and a travel time of 41m 51s and appears to belong near the H point[8] of core travel-time tables ($\Delta = 408°$). As far as I am aware, this is the first report of $PKKKP_{GH}$. In this region $d^2T/d\Delta^2$ is very high, which explains why the phase is visible at all.

The first thing to be said about these data is that PKKKP and PcP are both very short signals lasting less than 2 sec. PKKKP has a reversed polarity which possibly arises from double passage through a caustic in the core (a minimax reflection as described by Jeffreys and Lapwood[9]). This point needs further investigation. Nevertheless, it seems reasonable to assert that PKKKP and PcP represent a better view of the source than PKiKP. We can now compare these two phases for Milrow and Cannikin. No yields have been published for these events but they are presumed to have yields of 1 and 5 megatons, respectively. It is clear from Fig. I-7(a-b) that the time scales as well as the amplitude scales of the two PKKKP signals are different. However, the scaling is very much less than 5 to 1. The depths of burial of the two events were 4000 feet (Milrow) and 6000 feet (Cannikin) and the time scaling is roughly in this ratio, suggesting that depth of burial may have an effect. Unfortunately, it is difficult to sort out scaling owing to burial depth from scaling simply arising from explosion size, which will go as the cube root of yield. However, it is fairly clear from Fig. I-7 that the PcP and PKKKP signals both comprise more than one discrete pulse. Deconvolving the impulse displacement response with attenuation from the PcP signal yields a tentative source model for Milrow, shown in Fig. I-8(a-b).

Compare Fig. I-8 with the results of Frasier in Sec. A above. The agreement is remarkably close. We each conclude that the signal radiated to teleseismic distances consists of a primary pulse together with a complicated combination of a reflected pulse (negative) and a signal contributed by spalling (positive). The ground displacement beneath the shot thus appears from teleseismic data to contain an impulsive term together with a step function (not necessarily of the same size).

I wish to acknowledge Dr. E. A. Flinn (Teledyne-Geotech) for providing the Cannikin data.

D. Davies

C. SIZE OF EARTHQUAKES

The dimensions of the rupture region of an earthquake are difficult to acquire from seismic data. Even if the earthquake breaks surface in an accessible region, this gives no clear indication of whether the visible rupture length is the total length of activity and, of course, no guide at all to the depth of the ruptured region. Study of the area of aftershock regions has been used for large earthquakes.[10] Indirect methods have become popular in the last year or two, depending mainly on spectral observations of seismic signals, and the determination of a "corner frequency" which is related to the size of an earthquake. We propose a simple time-domain approach to the problem which so far has yielded interesting results.

It is assumed that an earthquake can be described as a plane region across which sudden rupture occurs. This rupture nucleates at a certain point on the fault plane and spreads over the plane until it is terminated by some unspecified obstacle. The rupture is often presumed to propagate with a velocity less than that of the shear wave velocity of the medium. Little is known about the "quenching" process by which the rupture is brought to a standstill. If this description of an earthquake is valid, the duration (τ) of the far-field radiated signal should bear a close relation to the size of the event. In particular, one would expect that by observation with P-waves having near-source velocity α

$$L\left(\frac{1}{v_R} + \frac{1}{\alpha}\right) \geq \tau \geq L\left(\frac{1}{v_R} - \frac{1}{\alpha}\right)$$

where L is the largest distance the rupture propagates with velocity v_R. The extreme (equal) cases correspond to a rupture propagating in the same or opposite direction as the P-wave. A reasonable upper bound to the largest dimension of the earthquake is then 2L, or typically 16τ kilometers. A more probable value if fault plane and rupture velocity vector orientation are random is 8τ kilometers. In the past, determination of τ (which clearly needs short-period seismograms) has been severely limited by the difficulties associated with short-period data. However, a digital array removes many of these difficulties and high-quality records are readily available. One problem remains – that lateral heterogeneities in the upper mantle, and particularly in the source region, lead to very confusing coda and do not allow a judgment to be made of where the signal ends and the coda begins. Here, the power of an array to beamform toward specified phases of an event can be used to advantage. Once an event has been chosen, several phases can be examined and the shortest in duration selected to give an estimate of τ. We find that core reflections are invariably the most useful for this purpose as the initial signal has emerged steeply from the heterogeneous zone.

In Fig. I-9(a-c), we give three examples; in each case, we show the P-wave and PcP-wave beams formed by LASA. In some instances, a surface reflection is also visible. It is clear that in no case is the signal in the ground at LASA of more than 1 sec in duration, from which we infer that the sources are at most 16 km in size and probably much smaller. Particularly striking is event (c). The signal looks exactly like the instrument response to a step function in displacement, and we propose that the dimensions of this deep earthquake are at most 4 km.

The difference in character of PcP among the three events is remarkable. It bears information on the time-domain response of the core-mantle boundary, and we are constructing a model consistent with these data.

D. Davies
A. M. Ziolkowski

REFERENCES

1. O. Kulhánek, "P-Wave Amplitude Spectra of Nevada Underground Nuclear Explosions," Pure Applied Geoph. 88, 121-136 (1971).
2. T. J. Cohen, "Source-Depth Determinations Using Spectra, Pseudo Autocorrelation and Cepstral Analysis," Geophys. J. R. Astr. Soc. 20, 121-136 (1971).
3. Seismic Discrimination Semiannual Technical Summary Report to the Advanced Research Projects Agency, Lincoln Laboratory, M. I. T. (31 December 1969), pp. 1-2, DDC AD-700322.
4. D. L. Springer and R. L. Kinnaman, "Seismic Source Summary for U. S. Underground Nuclear Explosions, 1961-1970," Bull. Seismol. Soc. Am. 61, 1073-1098 (1971).
5. Seismic Discrimination Semiannual Technical Summary Report to the Advanced Research Projects Agency, Lincoln Laboratory, M. I. T. (31 December 1970), pp. 19-21, DDC AD-718971.
6. D. L. Springer, "P-Wave Coupling of Underground Nuclear Explosions," Bull. Seismol. Soc. Am. 56, 861-876 (1966).
7. D. L. Bernreuter, E. C. Jackson and A. B. Miller, "Control of the Dynamic Environment Produced by Underground Nuclear Explosions," Symposium on Engineering with Nuclear Explosives, 14 January 1970, CONF-700101, 979-993, National Bureau of Standards, U.S. Department of Commerce.
8. B. A. Bolt, "Estimation of PKP Travel Times," Bull. Seismol. Soc. Am. 58, 1305-1324 (1968).
9. H. Jeffreys and E. R. Lapwood, "The Reflection of a Pulse Within a Sphere," Proc. Roy. Soc. (London) A. 241, 455-479 (1957).
10. R. C. Liebermann and P. W. Pomeroy, "Source Dimensions of Small Earthquakes as Determined from the Size of the Aftershock Zone," Bull. Seismol. Soc. Am. 60, 879 (1970).

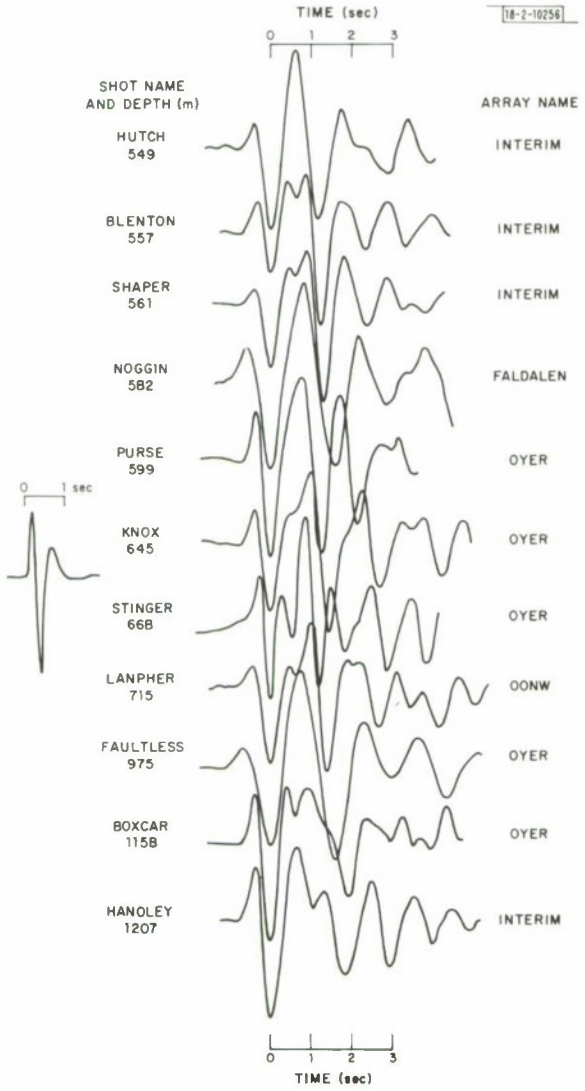

Fig. I-1. Eleven NTS P-waves recorded at arrays in Narway. Events are arranged by increasing depth in meters from top to bottom. To left af data is shawn shart-periad displacement response af seismameter, attenuated ta appraximate Earth's absarption fram NTS to Norwoy.

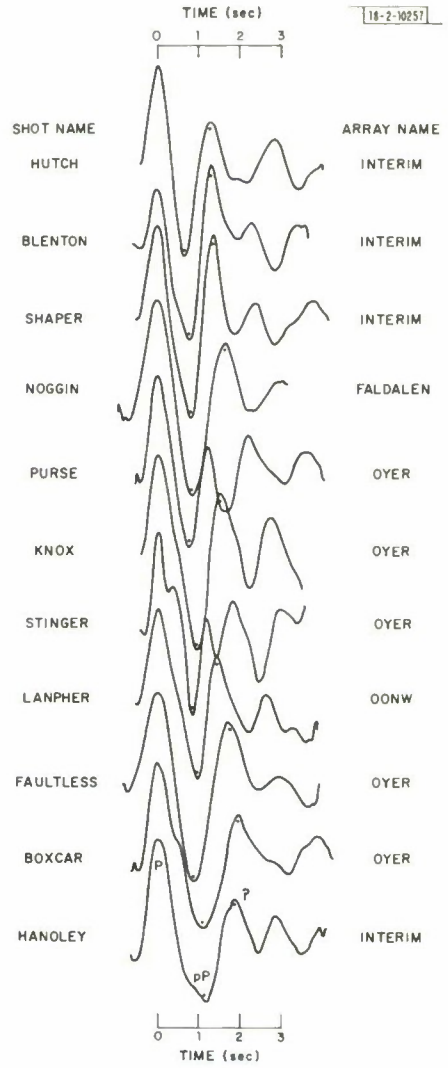

Fig. I-2. Deconvalved displacement recards af seismagrams in Fig. I-1. These waveforms are abtained by remaving instrument response fram data. First troughs are interpreted ta be pP-phases.

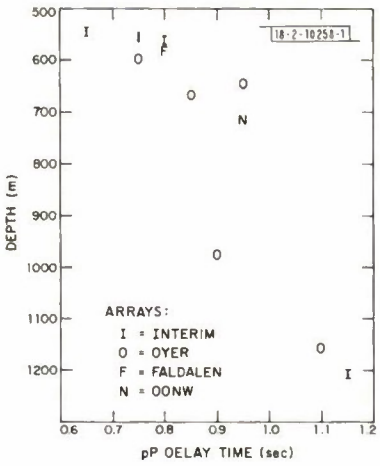

Fig. I-3. pP delay times vs depth for NTS events. These are obtained by inspection of Fig. I-2. Array recording each event is shown.

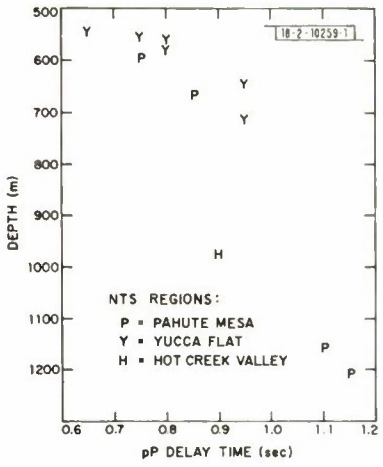

Fig. I-4. pP delay times vs depth for NTS events. NTS source region is indicated for each event.

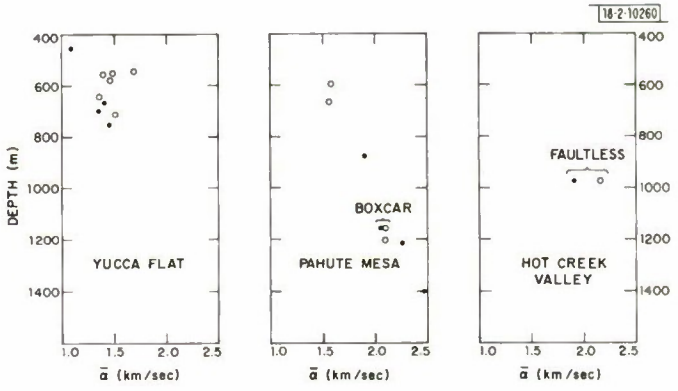

Fig. I-5. Comparison of average velocities at NTS regions obtained from pP delay times. Data obtained by Kulhánek from observed minima in amplitude spectra of NTS shots. Open circles calculated using delay times from reduced records of Fig. I-2.

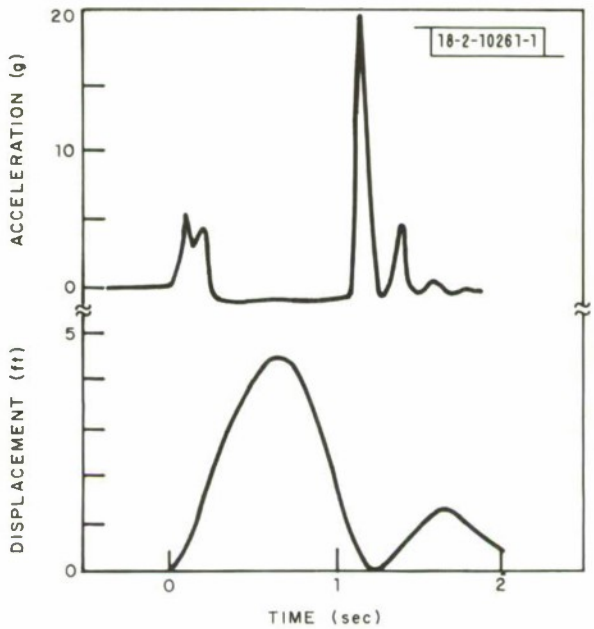

Fig. I-6. Surface acceleratian and displacement aver a "typical" cantained NTS explasian. Secand acceleratian peak accurs when rack material returns ta graund level after ~1 sec af free fall.

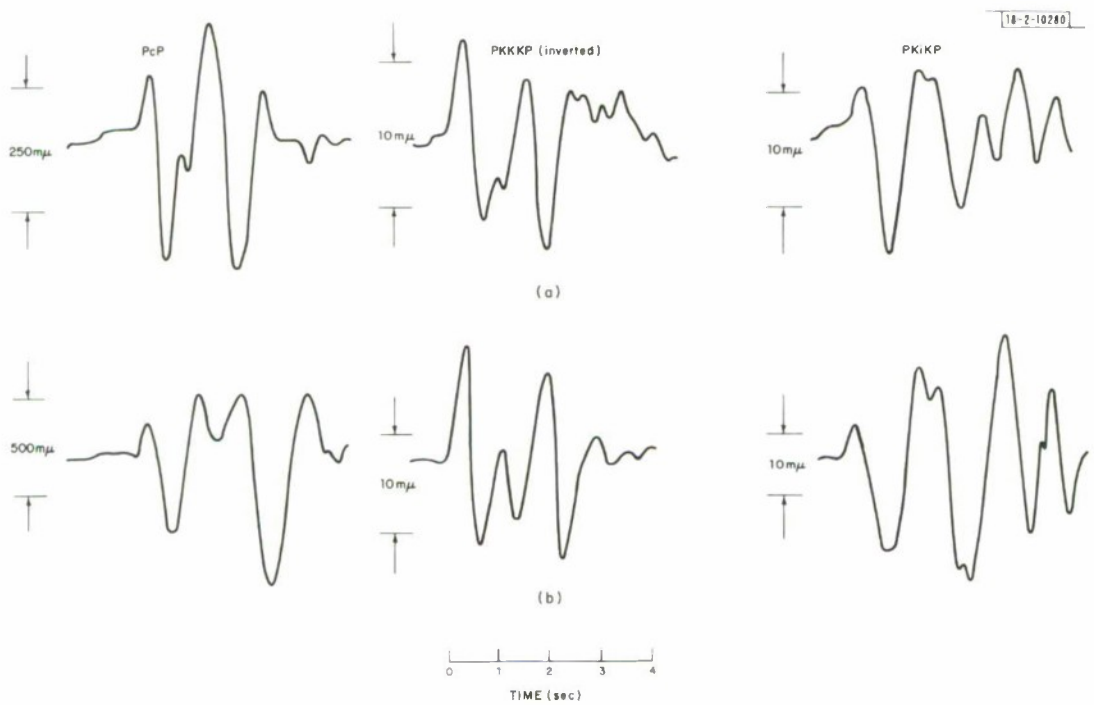

Fig. I-7. Core phases fram (a) Milraw and (b) Cannikin.

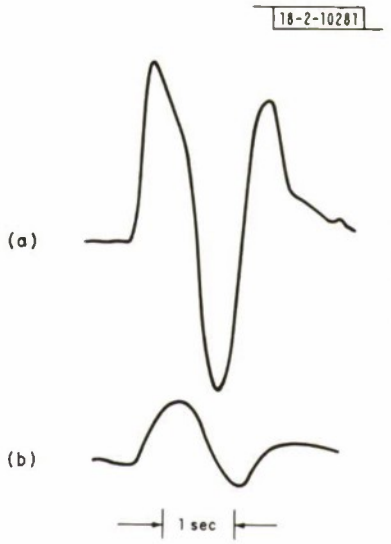

Fig. I-8. (a) Input function to LASA far PcP from Milrow; (b) neor-saurce displacement ta praduce this input functian.

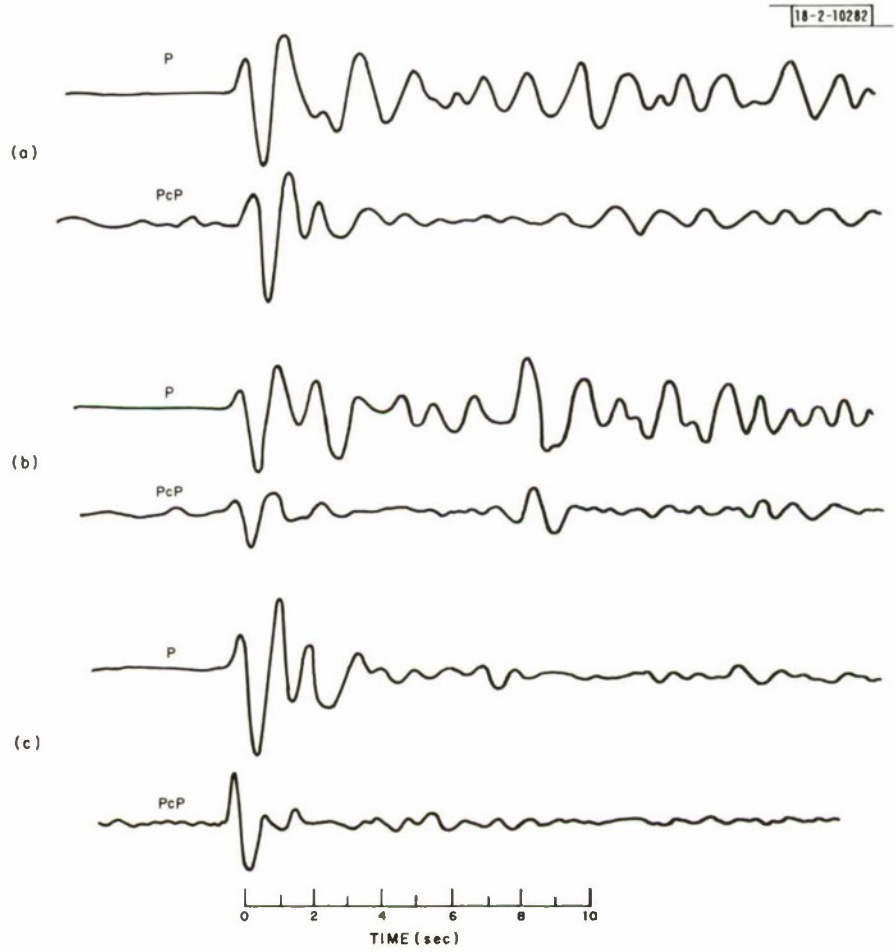

Fig. I-9. P- and PcP-wave beams farmed by LASA fram three earthquakes. (a) Kamondarsky Islands, 20 Januory 1969; h = 23 km, m_b = 6.1. (b) Komandarsky Islands, 4 April 1969; h = 27 km, m_b = 5.4. (c) Alaska, 10 June 1968; h = 182 km, m_b = 5.6.

II. PROPAGATION

A. NUMERICAL STUDIES OF SEISMIC WAVE PROPAGATION

A numerical integration technique has been developed† which solves the elastic equations governing coupled compressional and shear waves in inhomogeneous media. By neglecting doubly backscattered waves, the equations reduce to a set of first-order differential equations which are easily numerically integrated for media in which standard numerical techniques cannot be applied. For waves passing through a medium, the theory is valid provided that $(\omega/\alpha')^2 \gg 1$ and $(\omega/\beta')^2 \gg 1$, where ω is the angular frequency and α' and β' are the gradients of the compressional and shear velocities, respectively. The limits to which these high-frequency restrictions can be pushed are examined below.

In studies of seismic source functions, it is important to consider the effect of velocity and density transition zones in the Earth on short-period signals. As a test of the above technique, the plane-wave transmission response for a transition zone was calculated and compared with the discrete time solution,‡ which has been shown to converge to the exact continuous time solution. The transition layer is shown in Fig. II-1. Both velocity α and density ρ decrease linearly over a 2-km zone, and have end values which are typical for a crustal sedimentary layer over basement rock. Figure II-2 shows the discrete time transmission response of the transition to an incident delta function of compressional particle velocity with energy density 1. Three solutions are shown for discrete time intervals $\Delta\tau = 0.4$, 0.2, and 0.1, and are nearly identical at coincident sample points. The first arrival is a delta function of area ~0.99, followed by a smooth finite amplitude tail which is the accumulation of doubly backscattered multiples which travel forward and arrive after the first pulse. Such backscattering is neglected in the numerical integration scheme.

Figure II-3 shows the amplitude and phase response of the transmitted wave calculated by each method as a function of frequency. The crosses indicate the superposed discrete time solutions (all three are identical), and the circles show the numerical integration solutions. From the discrete solution, we see that the transmitted delta function makes the spectrum nearly flat except below 1 Hz, where the negative portion of the response in Fig. II-2 lowers the amplitude. The phase response is essentially 0. This verifies the assumption in the numerical integration scheme that backscattered reflections are practically negligible. For the transition model considered, $\omega/\alpha' \doteq 10$ corresponds to a frequency of ~1.6 Hz. Above this frequency, $(\omega/\alpha')^2 > 100 \gg 1$ and the numerical integration scheme gives results which closely match the discrete time solution. Below 1.6 Hz, the amplitude response of the numerical integration scheme falls off rapidly, as it should; however, the phase distortion remains less than 30°. This implies that time-domain seismograms can be synthesized from Fourier components of the transmission response without much distortion of the wave shape.

---

† T. E. Landers, "Elastic Waves in Laterally Inhomogeneous Media," Ph. D. Dissertation, Stanford University (1971).

‡ C. W. Frasier, "Discrete Time Solution of Plane P-SV Waves in a Plane Layered Medium," Geophysics 35, 197-219 (1970).

For geologic zones with less severe velocity gradients, such as the Moho, the numerical integration will be accurate across the complete short-period band.

Similar studies are being made on the coupled conversions of P- to S-waves in transition zones for both the transmission and reflection problems.

C. W. Frasier
T. E. Landers

B. SPECTRAL DISTORTION WITHIN SHADOWS

The effects upon seismic wave propagation of lateral variations in the Earth's structure have been investigated in several previous SATS using first-order ray theory, and it was found that for realistic models quite large amplitude anomalies and even shadows can be produced. However, ray theory is strictly applicable only in the limit, as the frequency tends to infinity. This means that the amplitude anomalies will be functions of frequency or, stated differently, that lateral variations can distort the spectra of seismic signals. Here we present some estimates of the magnitude of such effects for the case of a dipping high-velocity lithospheric slab beneath an island arc.

The method used consists of orienting the coordinate axes so that the velocity in the vicinity of the slab may be approximated as a function of one coordinate only (see Fig. II-4). The problem is thus reduced to one of reflection and transmission from a one-dimensional velocity variation, which is solved by direct numerical integration of the equations of motion resulting when the factor $\exp[i(\omega t - kx)]$ is removed.

Here we consider a symmetric model in which the two seismic velocities and the density are given by functions of the form $A + B \exp[-(z/h)^2]$. Such a restriction is not necessary; any variation at all can be handled by the method. Figure II-5 shows the calculated transmission coefficient as a function of wavelength for P-waves incident at a variety of angles upon a slab with a 10-percent velocity increase. Ray theory predicts perfect transmission for angles less than 64.4°, and total reflection for greater angles; thus, all the cases shown lie within the geometrical shadow. It is clear that the frequency above which ray theory applies is very roughly given by $\lambda = h$, but is a strongly varying function of the angle of incidence, particularly near grazing incidence. It is also clear that in a shadow zone a pronounced tilt will be introduced into the spectrum, which will be difficult to distinguish from the effect of anelastic attenuation. (The effect of attenuation on a plot such as Fig. II-5 would be a straight line passing through the upper left-hand corner.) The curve for $i = 71.0°$ in Fig. II-5 corresponds roughly to a value of t^* (T/Q, where T is travel time and Q is the effective quality factor) of about 6, for example.

Thus, not only magnitude measurements but also spectral measurements will be badly biased when shadowing occurs. This effect may, in fact, prove of value for determining the thickness of the descending lithosphere; current estimates run all the way from 20 to more than 100 km.

B. R. Julian

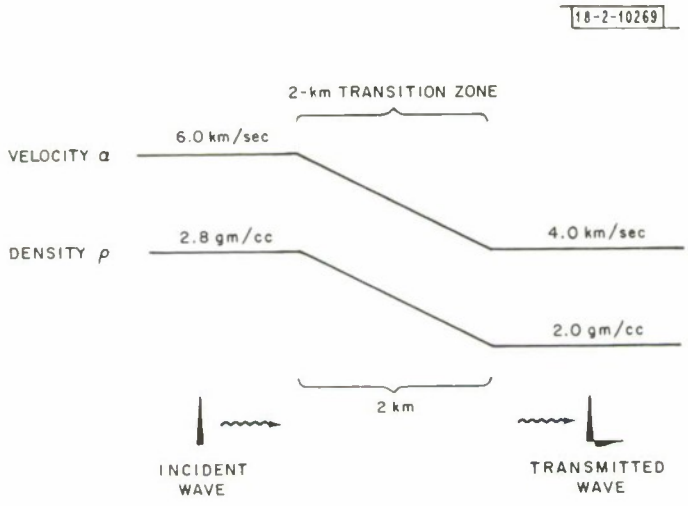

Fig. II-1. Tronsition loyer between two holf spaces. Incident P-wave is o delta function in higher-velocity half space. Transmitted wave emerges into lower-velocity half space.

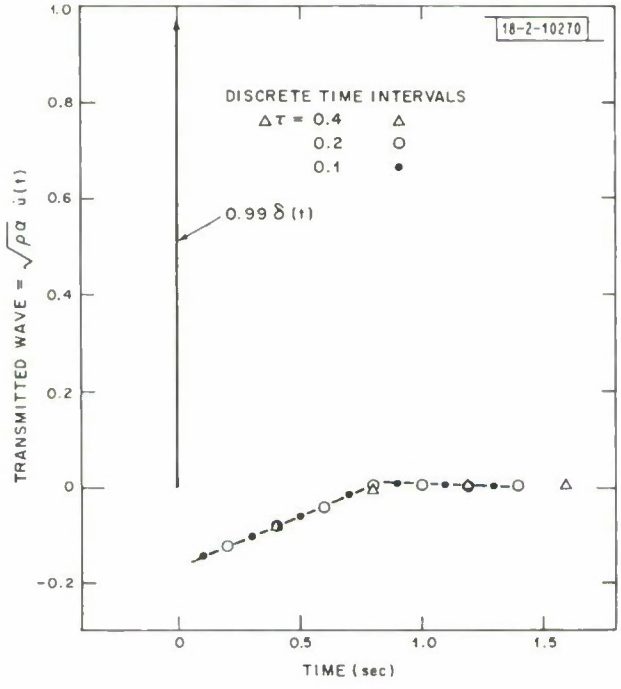

Fig. II-2. Discrete time salution for transmitted wove. Three different time increments $\Delta\tau$ give neorly identicol volues at coincident times. First spike hos oreo of ~0.99, and negotive toil hos areo of ~0.06.

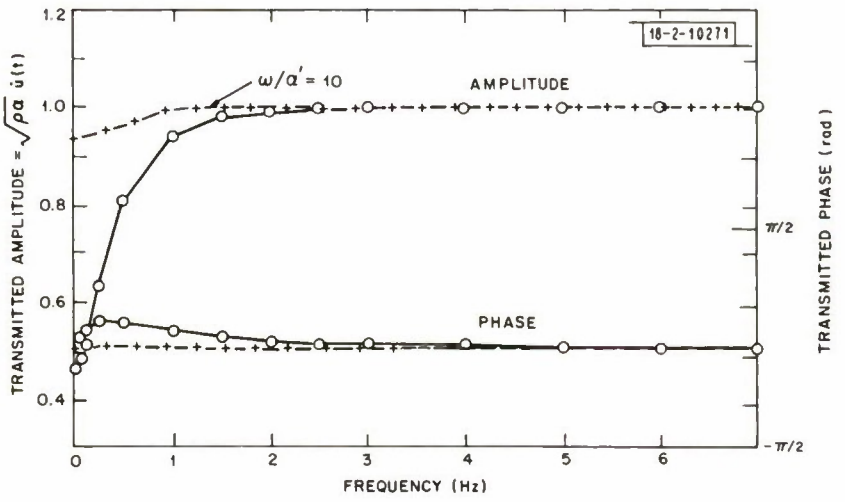

Fig. II-3. Comparison of transmission responses calculated by two methods. Circles are values obtained by numerical integration, and crosses show discrete time solution. For frequencies above $\omega/\alpha' = 10$, numerical integration method is quite accurate.

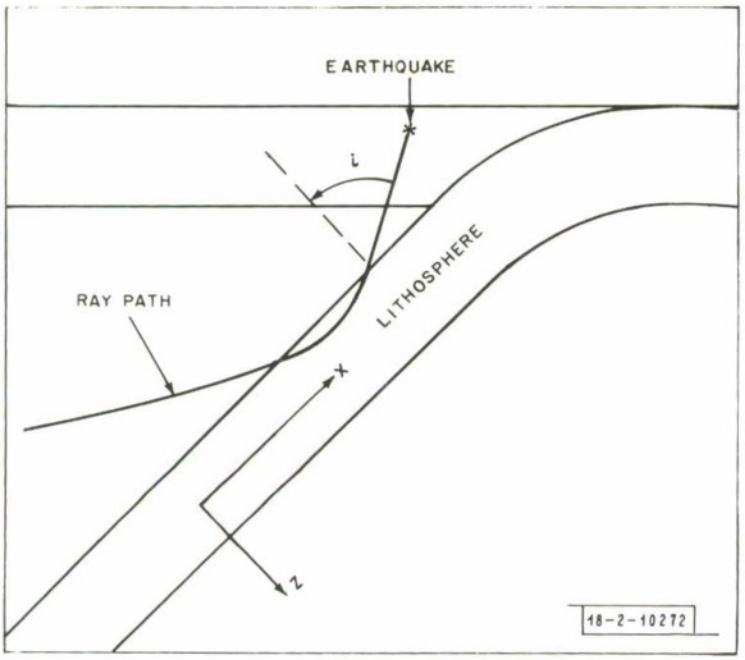

Fig. II-4. Schematic diagram af descending lithaspheric slab, shawing arientatian af caardinate system.

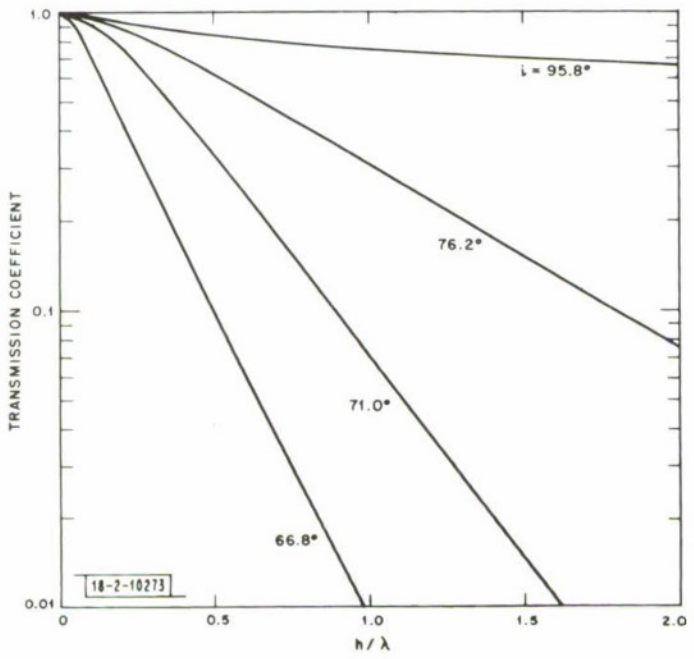

Fig. II-5. P-wave transmissian caefficient far slab madel with 10-percent increase in campressianal and shear velacity and na density change, as a functian af wavelength af incident wave far variaus angles af incidence. Critical angle in this case is 64.4°; h is the half-width af the slab (see text).

III. ARRAYS

A. ANALYSIS OF LONG-PERIOD MICROSEISMIC NOISE AT NORSAR

The analysis of microseismic noise is extremely important for the problem of seismic discrimination. This analysis provides the data to determine the deteetion capability of a seismic station, or array, for both short- and long-period signals. In addition, the analysis provides information concerning the character of the seismie noise. This information, in turn, can be used to determine the effectiveness of various signal-proccssing methods in reducing the noise power.

There have been several investigations[1-3] of the seismie noise field at LASA. These analyses have lent considerable insight into the nature of the microseismic noise field. We will now prcsent the results of analysis of the microseismic noise in the 6- to 40-sec period range at NORSAR. High-resolution frequency-wavenumber spectra[4] have been measured for the noise, as well as power spectra and cohcrencc.

Thc frcquency-wavenumber spectra of the long-period microseismic noise, in the 6- to 40-sec pcriod range, have bcen measured at the long-period array at NORSAR. This array eonsists of 22 scts of 3-component long-period seismometers loeated within an aperture of about 125 km. The beam pattern of the array in k-space is shown in Fig. III-1. The high-resolution method was employed, and the parameters of the measurement were the same as those used previously for the analysis of long-period noisc.[4] Five different noise samplcs were analyzed during a 1-month interval in Junc 1971. The results to be presented are typical of the entire set of data.

The results of one of the measurements for a 1 June 1971 noise sample are shown in Fig. III-2(a-c) for frequencies of 0.03, 0.04 and 0.05 Hz, respectively, as measured for the vertical instruments. The corresponding data for the north-south and east-west seismometers are shown in Figs. III-3(a-c) and -4(a-c), respectively. A typical power spectrum is shown in Fig. III-5. The method used to estimate the eoherenee and spectra is the same as that given previously.[3] The data in Fig. III-2(a-c) indicate that the 20- to 40-sec microseisms contain a component which consists of fundamental-mode Rayleigh waves whieh propagate from a wide range of azimuths. This fact is also corroborated by the data in Fig. III-3(a-e). The data in Fig. III-4(c) show that the noise also consists of fundamental-mode Love wavcs which arrive at the array from the same direction as the fundamental-mode Rayleigh waves. This indicates that the same mechanism may be responsible for the generation of both Rayleigh- and Love-wave microseismic noise at NORSAR.

The eoherence data show that the 20- to 40-sec microseisms also contain a nonpropagating component. The noise levels depicted by the power speetra in Fig. III-5 are typical of those found previously at LASA.[3]

J. Capon

B. SIMULTANEOUS ANALYSIS OF LONG-PERIOD MICROSEISMIC NOISE AT ALPA AND LASA

Thc long-period background seismic noise limits thc identification threshold at which the powerful M_s-m_b discriminant can be applied at LASA. This noise has been investigated[3] and

found to eonsist of two eomponents. One component propagates across LASA as a fundamental-mode Rayleigh wave and is believed to be caused by the action of surf on coastlines. The other component is nonpropagating (or ineoherent) noise, and data have been obtained that indieate it is eaused by atmospheric pressurc fluctuations. This component always provides a significant eontribution to the total noise power.

The previous analyses were able to obtain only the direetion of arrival at LASA of the propagating eomponent of the noise. Thus, it was not possible to determine the origin of these surface waves. Such a determination would be possible by obtaining the direetion of arrival of these surface waves simultaneously at two arrays located reasonably elose to eaeh other. This measuremcnt has beeome feasible to perform as a eonsequence of the availability of data from the Alaskan Long-Period Array (ALPA).

The ALPA is an array of nineteen 3-eomponent long-period seismometers arranged 20 km apart in a filled hexagonal pattern of about 80-km diameter. The eenter of the array is loeated about 50 km north of Fairbanks, Alaska. The beam pattern of the ALPA is depieted in Fig. III-6 where it is seen that there is a serious aliasing sidelobe whose magnitude is only 1 dB less than that of the mainlobe. This severe sidelobe problem is due to the almost perfect periodieity in spaee of the seismometers arrangcd in the filled hexagonal pattern. This sidelobe is loeated at a distanee, in wavenumber spaee, from the mainlobe of about 0.057 Hz/km. Thus, there eould be serious problems in beamforming or frequeney-wavenumber analysis of surfaee waves with a period of $1/0.5 \times 0.057 \times 3.7) \cong 10$ see. This eould be a serious problem for seismie discrimination using the M_s-m_b criterion, sinee Rayleigh waves observed at short distanees from their origin often have their dominant energy at the shorter periods, sueh as in the 10- to 14-sec period range.

The high-resolution frequency-wavenumber speetra,[4] eoherenee and power speetra of the noise in the 6- to 40-sec period range were measured simultaneously at ALPA and LASA for time periods during the days 16 September, 25 September and 20 Oetober 1970. The results for two of these time periods are shown in Figs. III-7 and -8. The directions shown in these figures pertain to seismie noise in the 20- to 25-sec period range and were obtained from the frequency-wavenumber spectra results for the vertieal, north-south and east-west arrays at both ALPA and LASA. In Figs. III-7 and -8, we see that the loeation of the noise source extends over a wide region of the earth. In addition, this region contains a low-atmospherie-pressurc area. The loeations of these areas were obtained from surface eharts showing isobars and low- and high-pressure regions. Thus, the results of Figs. III-7 and -8 show that the souree of the seismic noise ean bc assoeiated with the existenee of low-pressure atmospheric disturbances near eoastlines, as indicated by Haubrieh and McCamy.[2] The results for the 25 September 1970 noise sample did not yield a loeation of the noise souree whieh eould be assoeiated with a low-pressure region.

The power speetra of the 16 September 1970 noise, for the vertieal, north-south and east-west seismometers at site 2-4 at ALPA and site A0 at LASA, are shown in Figs. III-9(a) and (b), respectively. These data show that the seismie noise levels at ALPA and LASA are eomparable. Similar results were obtained for the other two noise samples that were analyzed.

J. Capon

C. DISCUSSION OF A SUITE OF LONG-PERIOD SIGNALS RECORDED IN NORWAY FROM ASIAN EVENTS

Lincoln has reeeived a limited set of long-period digital recordings from the eompleted NORSAR and a set of plots of vertieal instruments for four events from Central Asia. Only one well-reeorded event from the area has been found on the digital tapes. Data from these five events have been eombined with recordings of thirteen additional 1968 events obtained during the noise-survey stage of NORSAR to make some preliminary observations eoneerning the events, the site and M_s-m_b discrimination procedures. Figure III-10 shows the loeation of the eighteen events in this study and Table III-1 gives more detailed information eoneerning the individual events.

The 1968 data eame from sites identified as Oyer, Trysl and Faldalen. The Oyer site has now beeome subarray 01C. The Faldalen site was near subarray 07C, and Trysl was outside the eurrent NORSAR to the east and slightly north. The current NORSAR geometry and site nomenclature are shown in Fig. III-11.

Figure III-12 shows long-period vertieal Rayleigh waves reeorded at all sites in NORSAR. Earthquake 8 and presumed explosion 3 show a relatively well-developed phase with a period on the reeord of about 14 see. This signal is the burst of higher frequeney whieh is followed by lower-frequeney arrivals. We note in passing the strong similarity of signal shape between these two events. Since the paths are similar, this suggests long-period exeitation with similar-shaped speetra for these two events. Event 10 has only the slightest hint of this 14-see signal, although the path is again not very different. Though this eould be due to path effects, it is more likely that the source is rieher in the lower frequeneies so the 14-see signal has a relatively smaller eontribution. There is no hint of the 14-see signal for event 2. The burst of largest signal is at about an 18-see period and may eorrespond to a flat portion of the group veloeity curve (see Filson's eomments on group veloeity in See. D below).

Event 3 shows a very interesting fact about the 14-see phase. Specifically, note that its contribution, relativc to other periods, is mueh less at sites 01C and 02C than at many others. In fact, there is a strong tendency for it to be weak in the northwest part of the array. The effeet is strong for a relativcly small change in rceeiver site.

Figure III-13 shows Raylcigh and Love signals for the remaining events. The vertical, north-south, and east-west eomponents are shown for eaeh event. Note that data werc obtained only from the Oyer site for many of these events so that the high-frequeney eomponent is expected to be relatively small or shifted slightly to longer periods.

The data have been analyzed to obtain measurements of surfaee-wave magnitude using both Rayleigh and Love waves. The results are tabulated in Table III-1. Figure III-14(a) is a plot of Rayleigh-wave M_s vs the NOS m_b values. M_s was computed from $M_s = \log(A/T) + 1.66 \log \Delta$, where A is peak-to-peak signal in millimierons, Δ is distanee in degrees, and T is period in seeonds. The period was restrieted to the 18- to 23-see band. The same formula was used for Love waves but thc largest signal with $T \geqslant 18$ was used. These data are shown in Fig. III-14(b).

Love waves reeeived from explosions at a reeeiver are usually smaller than the Rayleigh waves, but there is a reasonable number of earthquakes for whieh this is not true. Thus, if the largcr of the Rayleigh and Love M_s values is plotted vs m_b, the separation should be improved over a customary M_s-m_b plot sueh as Fig. III-14(a). This has been done in Fig. III-14(c) and,

TABLE III-1

NORSAR EVENT LIST

Event No.	NOS Data						Azimuth from NORSAR (deg)	Distance from NORSAR (deg)	Recarding Locatian Displayed
	Date	Origin Time (GMT)	Latitude (°N)	Langitude (°E)	Depth (km)	m_b			
1	21 July 68	01:41:19	55.2	113.3	33R	5.1	47.7	49.2	Oyer (01C)
2	24 August 71	16:33:22	52.2	91.4	N	5.2	63.8	42.6	Array (Z anly)
3*	25 April 71	03:32:58	49.8	78.1	OR	5.9	75.4	38.2	Array (Z anly)
4*	19 June 68	05:05:57	49.9	79.1	OR	5.5	75.4	38.2	Oyer (01C)
5	14 March 68	02:08:37	42.3	66.5	33	5.4	93.3	37.9	Trysl
6	13 March 68	22:38:39	42.4	66.5	33	5.2	93.2	37.8	Trysl
7	15 June 71	22:04:13	41.5	79.3	N	5.6	83.2	44.7	01C
8	23 March 71	20:47:17	41.5	79.3	N	6.0	83.2	44.7	Array (Z only)
9	20 July 68	08:22:08	39.4	73.8	61	4.8	89.7	43.7	Oyer (01C)
10	3 May 71	00:33:22	30.8	84.5	16	5.4	87.3	55.8	Array (Z only)
11	11 February 68	20:38:29	34.2	78.6	44	5.1	89.9	50.1	Oyer (01C)
12	21 March 68	02:45:56	37.8	72.5	131	4.8	92.3	44.3	Oyer (01C)
13*	21 May 68	03:59:11	38.9	65.2	13	5.4	98.0	39.9	Oyer (01C)
14*	1 July 68	04:02:02	47.9	47.9	33	5.5	104.5	24.8	Oyer (01C)
15	11 May 68	12:12:41	41.0	49.8	15.6	5.0	112.0	30.9	Oyer (01C)
16	15 July 68	08:33:37	32.5	48.7	33R	4.6	121.6	37.5	Oyer (01C)
17	13 May 68	02:46:35	43.5	40.3	5	5.1	121.0	24.7	Oyer (01C)
18	27 February 68	13:37:43	39.5	25.4	30	4.7	150.2	23.3	Faldalen (07C)

TABLE III-1 (Continued)

Event No.	Log (A/T) Rayleigh†	Log (A/T), T Love‡	$M_{s(20)}$ Royleigh	$M_{s(T)}$ Love T ⩾ 18	M_s LASA Z Chirp if Available
1	2.01	1.4, 23	4.82	4.21	
2	–	–	–	–	
3	–	–	–	–	
4	0.93	Too small, <0.71, 20	3.55	<3.33	<3.22
5	2.13 ⓐ	1.47, 25 ⓔ	4.74	4.00	4.23
6	1.79 ⓑ	Too small, <1.0, 25 ⓕ	4.40	<3.61	3.99
7	–	–	–	–	
8	–	–	–	–	
9	1.01	0.77, 23	3.73	3.49	
10	–	–	–	–	
11	1.86	2.17, 25	4.67	4.98	
12	1.30	1.23, 22	4.02	3.95	
13	1.23? Interfering Event	<0.83, 20	3.89	<3.49	<4.34
14	1.13 ⓒ	0.70, 20 ⓖ	3.44	2.91	3.57
15	0.97	0.67, 30	3.45	3.15	3.64
16	1.38	1.46, 30	3.98	4.06	
17	2.28	2.45, 22	4.59	4.76	4.81
18	1.07 ⓓ	1.59, 18	3.36	3.88	

– No obsolute levels of 1971 data are given due to lack of certain colibration data for our topes.
* Presumed explosion.
† Largest peak-to-peak signal on vertical with A in millimicrons and T in seconds.
T limited to 18- to 23-sec range.
‡ Based on largest output from instrument in the range T ⩾ 18 sec.

ⓐ 2.79 at 15 sec
ⓑ 2.46 at 15 sec
ⓒ 1.99 at 15 sec
ⓓ 1.96 ot 14 sec
ⓔ 2.23 at 15 sec
ⓕ 1.99 at 15 sec
ⓖ 1.40 at 15 sec

} Signal maximum from instrument at lower frequencies for these events.

although the population is limited, we do see some improvement. The procedure makes sense theoretically as well as experimentally since the Rayleigh and Love radiation patterns from earthquakes are 45° out of phase, thus a strong Love wave may be received with a weak Rayleigh wave even if the actual generation of Rayleigh and Love waves is not anomalous. Since horizontal noise at NORSAR is often as small as the vertical, this use of Love waves is quite promising.

Two events – one presumed explosion and one earthquake – could be problems with these M_s-m_b data. These are events 13 and 15 and neither was affected by taking the larger of the Love and Rayleigh M_s values. Both of these events, as well as five other events of those with M_s-m_b values on Fig. III-14, were included in a previous LASA experiment.[5] M_s values or bounds from that experiment are also included in Table III-1. Figure III-14(d) is an M_s-m_b plot using the largest of the two NORSAR M_s values or the LASA value for M_s. The plot is unchanged from Fig. III-14(c) except that earthquake 15 has been raised slightly. The improvement is not large but encourages us to pursue such extremum methods more thoroughly. Our motivation in taking the maximum over stations is that earthquakes should have a more azimuthally variable radiation pattern than explosions, and separation may thus be improved over using simple averages. Of course, using maxima will require careful application of path corrections and learning systematic effects other than radiation patterns which could cause a station to have a high value of M_s. This has not really been done here in combining the LASA and Norway data. The point is to develop a procedure which will differentially augment M_s values for earthquakes and explosions with the larger increase for earthquakes.

There was an m_b 5.5 event at 04:11:24.7 at 41.1°N 143.5°E which caused problems at LASA, and perhaps at NORSAR, for event 13. The Rayleigh waves from this other event arrived at LASA at almost the same time as those from event 13, and made it impossible to get an M_s measurement. At NORSAR, the P arrived at about the time of Love waves from event 13. The P can be seen by checking polarization on Fig. III-13. The Rayleigh wave for event 13 at NORSAR looks acceptable but it is at the same time as PP from the interfering event. This could account for the high M_s value, but is not likely.

It is interesting to note that event 15 was identified as problem event H in the earlier LASA report[5] in which the event was discriminated by LASA M_s-m_b, although it did have a somewhat small M_s value.

R. T. Lacoss

D. INITIAL DISCRIMINATION RESULTS AT NORSAR

An initial study has been made of the detection and classification capabilities of NORSAR using the body-wave-to-surface-wave-magnitude (m_b-M_s) criterion. The chief purpose of this study is to identify lines of future research in discrimination procedures using NORSAR data.

The major difficulty in applying the m_b-M_s criterion is the measurement of surface-wave amplitudes of events presumed to be underground explosions – the presumption being based on body-wave detections and location. By using an array, the most simple way to increase the signal amplitude with respect to the noise field is to align the traces in time and sum; this sum or beam can then be used for the measurement of surface-wave amplitudes if the noise is sufficiently suppressed. In this study, beamforming is the main technique used in signal enhancement. In order to apply this technique, especially for weak signals that cannot be discerned on single

traces, one must have some idea of the rate of propagation of energy from the source region to the array site (i.e., the group velocity along a given path) and the rate of propagation of energy across the array (i.e., the phase velocity at the array site). Additionally, once the beam is formed, it is desirable to know how much signal loss is to be expected from the beamforming process. Because of the dispersive nature of surface waves, all these quantities are a function of period and propagation path; here, I have concentrated on the 20-sec components from sources in central Asia.

Figure III-15 shows a suite of Rayleigh-wave group-velocity measurements made at NORSAR from four events at a distance of about 40° and an azimuth of about 75°. A clear minimum at about the 18-sec period, typical for continental regions, is evident and 3.0 km/sec has been taken as a characteristic of the 20-sec group. Phase-velocity measurements at NORSAR are somewhat less precise because of the limited areal extent of the array (100 km). The high-resolution frequency-wavenumber technique was applied to two events from central Asia. The scatter is quite serious, but 3.5 km/sec has been taken as an appropriate velocity to be used in aligning the 20-sec portions of the Rayleigh-wave recordings. It is noted here that the direction of approach as yielded by the high-resolution technique was always within 10° of the computed direction for these sources and at most periods between 10 and 50 sec, within 5°.

With these velocities and using computed great circle azimuths, we can proceed to investigate the effects of beamforming on the Rayleigh-wave recordings. Figure III-16(a) shows the vertical motion of the Rayleigh waves from a presumed explosion in Eastern Kazakh on 25 April 1971. The traces have been aligned and summed and the beam is shown as the topmost trace. In this figure, the nature of the group velocity curve is seen, the initial long-period energy is followed abruptly by the shorter-period components which are, in turn, followed by 20-sec arrivals. Qualitatively, as seen on the beam, the 20-sec arrivals have been enhanced relatively to shorter periods due to the beamforming process. Figure III-16(a) quantifies this observation; here, the power spectrum of the beam is compared with the average spectrum of the 14C-ring long-period vertical sensors. These instruments are evenly spaced around the 300-km circumference of this outer ring. The spectra are computed using 512 points sampled at 1-sec intervals and are smoothed by taking the average of all components in a 0.01-Hz band. In the right-hand side of Fig. III-16(b), the difference between the beam and the average spectrum is plotted and it is seen that in this single case, when we have a high signal-to-noise ratio, the beam spectrum is down relative to the array by about 2 dB at 20 sec. At frequencies higher than 0.2 Hz, the beam spectrum is down in the range 10 to 15 dB below the array average. By assuming that the signal contains no energy at these higher frequencies, this can be considered the noise-suppression capability of the beam in this example. In any case, the signal deterioration of 2 dB (0.1 of a magnitude unit) at 20 sec caused by beamforming these traces is the relevant factor that will be applied to subsequent beams.

As an additional example of the beamforming capability, Fig. III-17 shows the aligned traces and beam for another presumed explosion from the same region as the example of Fig. III-16(a). Although the signal-to-noise ratio here is much smaller than in the previous example, we feel that a reliable M_S is measurable from the beam even though the arrival is not discernible on the individual traces.

A preliminary investigation has been made of one other signal-enhancement technique during this study. Figure III-18 shows the same event as Fig. III-16(a). However, in this case the second trace from the top has been replaced with a 180-sec portion of the top trace which is the beam. The second trace was then cross-correlated with the top trace, and the third trace represents the results of this cross-correlation. Although 180 sec is relatively short, an experiment has shown that doubling the length of the reference trace (in this case to include the low-amplitude long-period displacement) increases the maximum amplitude of the cross-correlation function by only 10 percent. This same reference trace of Fig. III-18 was applied to an event from the same region but in a case where I would decline to measure an M_s for the array beam. This beam is shown in Fig. III-19, beneath it the reference trace of Fig. III-18, and beneath that the cross-correlation function of the two. It is clear from the latter that a detection has been made and the amplitude can be measured with some confidence. The left-hand margins of Figs. III-18 and -19 are delayed equally with respect to the origin times of the individual events.

The M_s-m_b criterion has been applied to 18 earthquakes from central Asia and 9 presumed Kazakh explosions. The events considered are at distances between 32° and 64° to the northeast of NORSAR. The formula

$$M_s = \log_{10}(A/T) + 1.66 \log(\Delta) + 3.3 \qquad \text{(III-1)}$$

was applied to the vertical component of the Rayleigh wave, where A is the maximum amplitude in microns at period T, and Δ is the distance in central angle degrees. In this study, A was measured at periods within 2 sec of 20 sec. With the exception of 3 earthquakes, all the m_b values were taken from the NOS's Preliminary Determination of Epicenters (PDE) publication for events having depths less than 38 km or reported as "normal" depth. In Fig. III-20, the results of plotting M_s vs m_b are shown. The magnitudes of the earthquakes numbered 8, 14 and 15 are taken from the daily bulletin of the Seismic Array Analysis Center (SAAC). In Fig. III-20, we have plotted the empirical M_s-m_b relation of Gutenberg and Richter,[6] which is $M_s = 1.59\, m_b - 3.97$.

Although 0.1 of a unit of surface-wave magnitude has been added to all M_s values based on beam measurements, this correction will not affect the separation of source types that has been achieved in Fig. III-20. The M_s of explosion point 9 was measured from the cross-correlation function of Fig. III-19. The most surprising aspect of the figure is the apparent steepness of the fairly well-defined line the explosion points represent. Equation (III-1) was applied to earthquakes recorded at NORSAR for which NOS had reported an M_s, and the two agreed within 0.2 of a unit. It is difficult to attribute the slope of the line to a propagation-path effect since all these explosion surface waves had essentially the same path to NORSAR. Therefore, assuming that the NOS m_b determinations are consistent and these M_s measurements are accurate, the steep slope of the explosion line must be attributed to a source effect. The implication is that the short- and long-period displacements at the source do not scale equally with yield.

Explosion data from the Ural Mountains region have not been discussed here since they fall within a range where the direct application of Eq. (III-1) is not valid, and at present there is not a significant population of earthquakes against which to test. This should be a line of further research. It is impossible to make any general valid statements about the capability of an array after such a short study. However, one point becomes evident; using elementary techniques of data processing described here, the lower threshold of surface-wave detection has not been

reached when working with events near the lower threshold of NOS-reported location capability in central Asia. In order to establish the ultimate long-period capability of NORSAR, other reliable means of short-period detection and location of events in central Asia must be used or developed.

J. R. Filson

E. LASA HIGH-VELOCITY CORRECTIONS

One problem that has always plagued beamforming with LASA is the large time anomalies that exist within the array. Without sufficient knowledge of these corrections, it would not be possible to obtain correct or maximum beams. The time corrections for the short-period P-phase were determined some time ago and have been in use for several years. Only recently has emphasis been placed on beamforming for higher-velocity phases such as PKP or core phases such as PKiKP or PKJKP. The earlier analysis of the LASA time anomalies indicated that the core-phase corrections were large, often larger than the P-wave anomalies. With the aid of data obtained from IBM-SAAC and NOS,[7] these high-velocity corrections have been determined and are now in use in our PDP-7 beamforming programs.

The initial data contained about 200 core phases that were processed by the event processor at SAAC. One of the outputs of the event processor is a list of measured delay times for the phase as seen at LASA. These measured times were compared with the computed plane-wave times for the phase to yield the plane-wave anomalies which were tabulated into cells that cover each 10° in azimuth and 0.02 sec/deg in slowness. In the range of interest, 0 to 4 sec/deg, most cells did not contain any data points. It was necessary to approximate these data with a function which could then be evaluated at each cell. Earlier experience with the P-wave corrections indicated that the time anomalies could be approximated by a two-term Fourier series with azimuth.[8] Further, the core anomalies seemed to have a second- or third-order polynomial dependence with distance (slowness).

Defining the station correction as a two-term Fourier series in azimuth and a third-order polynomial in slowness meant that some twenty coefficients were necessary to express the function. However, when the condition is imposed that requires the function to be a constant (independent of azimuth) for zero slowness, the number of coefficients reduces to eleven. All data for each subarray have been least-square fitted to the restrained function defined by using the eleven coefficients. The resulting equation was evaluated at each cell point and compared remarkably well with the original data. Each cell point now had a data value obtained either from real data or from the equation. In order to obtain a more uniform table of values, the table was smoothed, requiring that the real data points would remain unchanged while the function values could change. The resulting tables of high-velocity LASA station corrections are now in use in all beamforming programs and are yielding excellent results, as indicated in the successful search for the core-phase PKJKP described in Sec. VII.

R. M. Sheppard

REFERENCES

1. R.T. Lacoss, E.J. Kelly and M.N. Toksöz, "Estimation of Seismic Noise Structure Using Arrays," Geophysics 34, 21-38 (1969), DDC AD-688564.
2. R.A. Haubrich and K. McCamy, "Microseisms: Coastal and Pelagic Sources," Rev. Geophys. 7, 539-571 (1969).
3. J. Capon, "Investigation of Long-Period Noise at the Large Aperture Seismic Array," J. Geophys. Res. 74, 3182-3194 (1969), DDC AD-671509.
4. J. Capon, "High-Resolution Frequency-Wavenumber Spectrum Analysis," Proc. IEEE 57, 1408-1418 (1969), DDC AD-696880.
5. R.T. Lacoss, "A Large-Population LASA Discrimination Experiment," Technical Note 1969-24, Lincoln Laboratory, M.I.T. (8 April 1969), DDC AD-687478.
6. B. Gutenberg and C.F. Richter, "Magnitude and Energy of Earthquakes," Ann. Geofis. 9, 1-15 (1956).
7. E.R. Engdahl and C.P. Felix, "Nature of Travel-Time Anomalies at LASA," J. Geophys. Res. 76, 2706-2715 (1971).
8. R.M. Sheppard, Jr., "Values of LASA Time Station Residuals, Velocity and Azimuth Errors," Technical Note 1967-44, Lincoln Laboratory, M.I.T. (8 September 1967), DDC AD-662004.

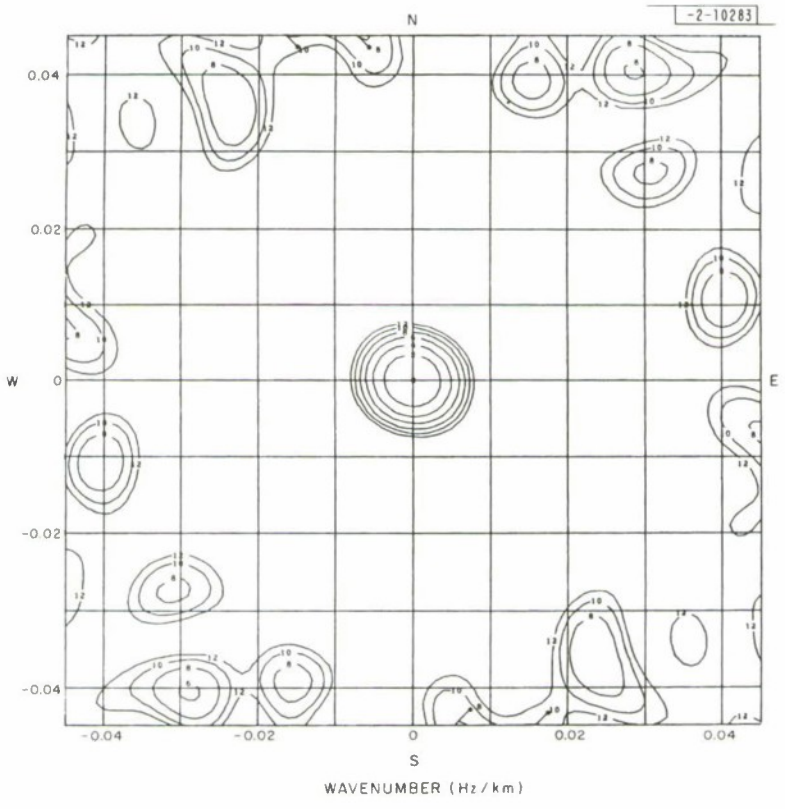

Fig. III-1. Beam pattern for long-period array at NORSAR.

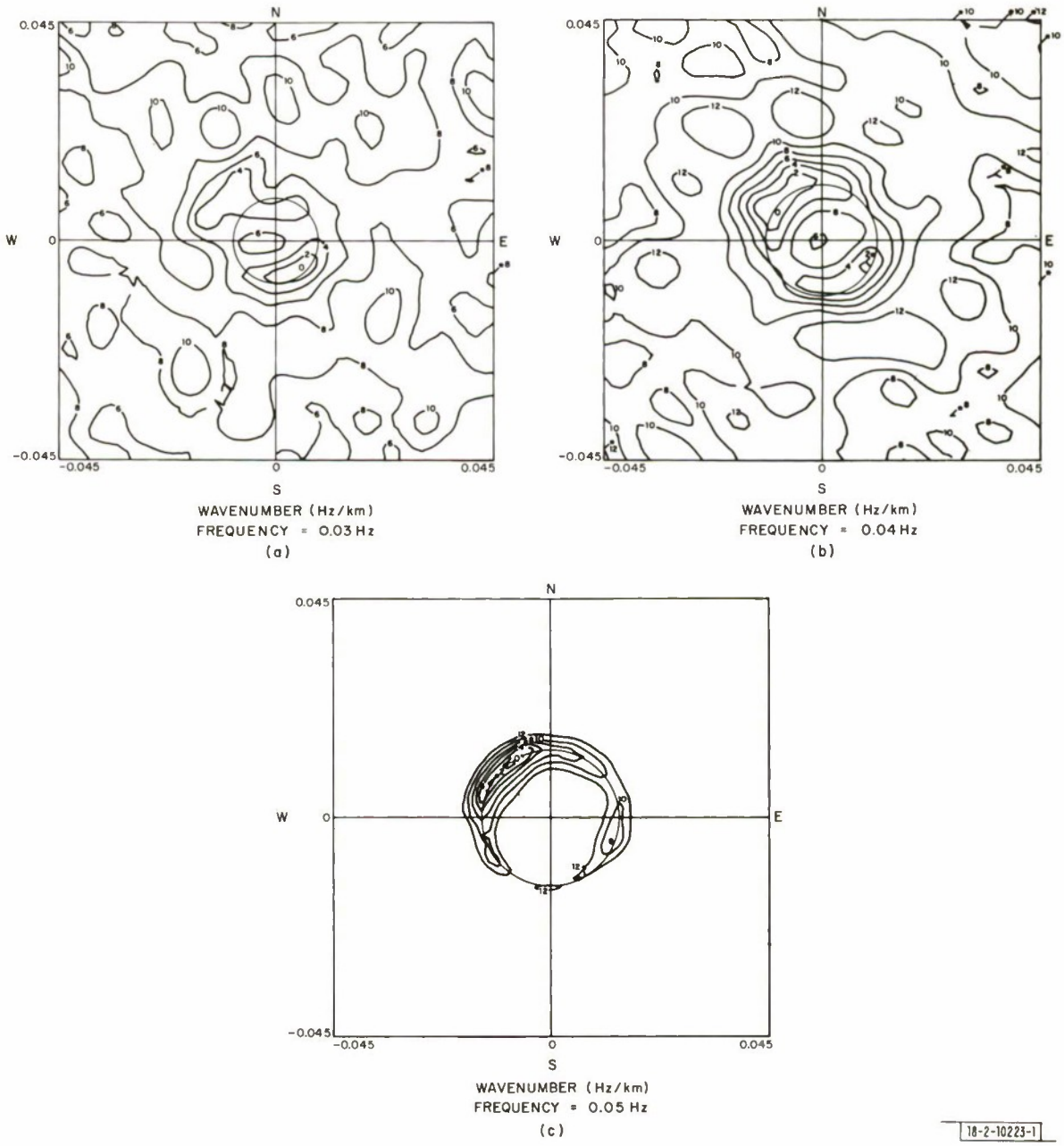

Fig. III-2(a-c). High-resolution frequency-wavenumber spectra for LPZ noise sample at NORSAR.

Fig. III-3(a-c). High-resolution frequency-wavenumber spectra for LPNS noise sample at NORSAR.

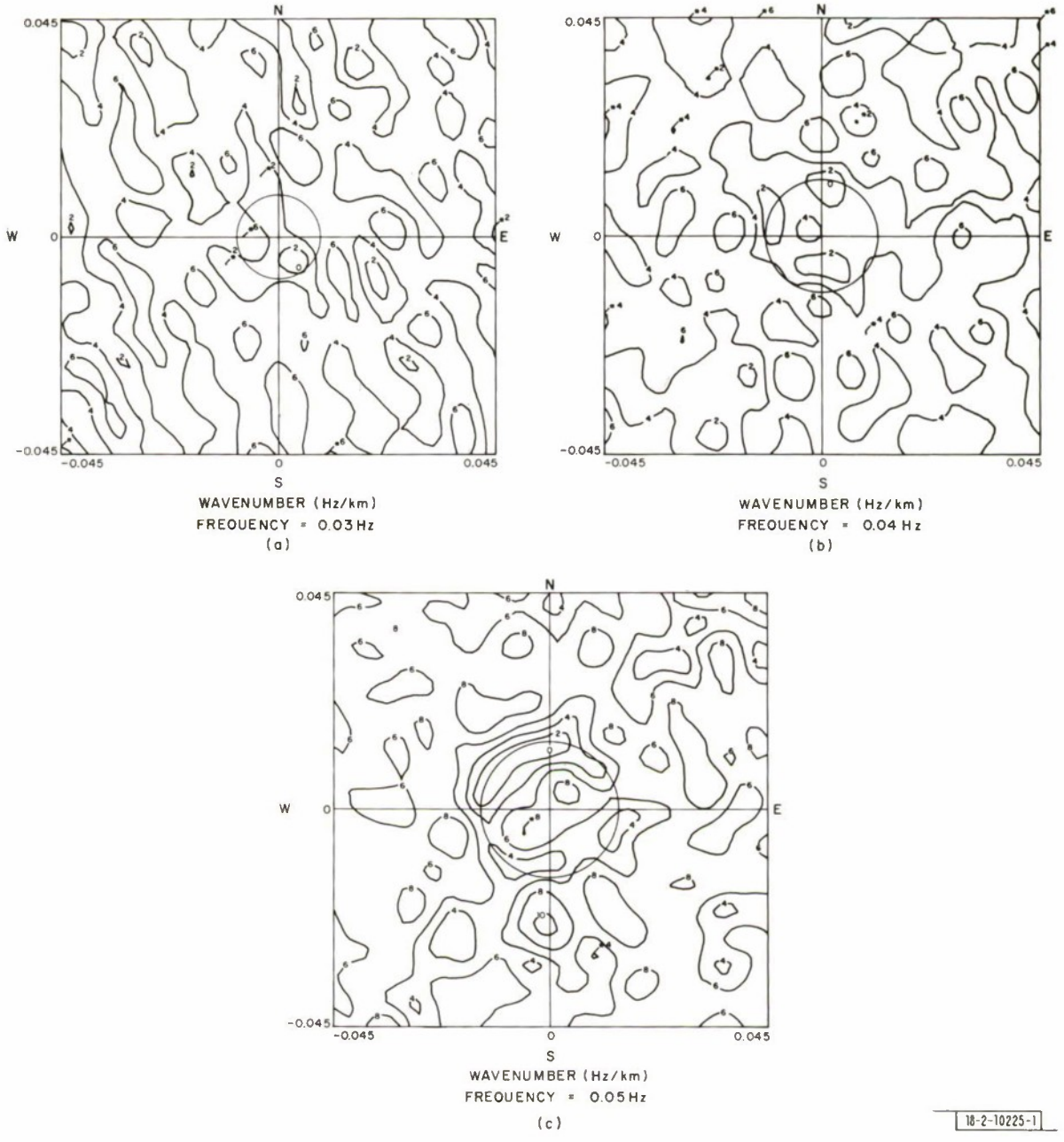

Fig. III-4(a-c). High-resolution frequency-wavenumber spectra for LPEW noise sample at NORSAR.

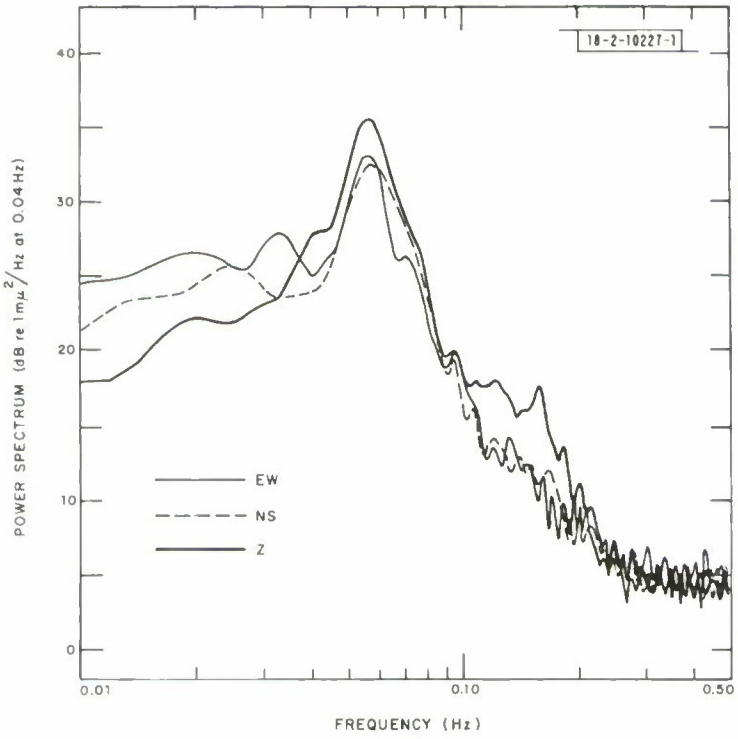

Fig. III-5. Power spectra for long-period noise sample at NORSAR.

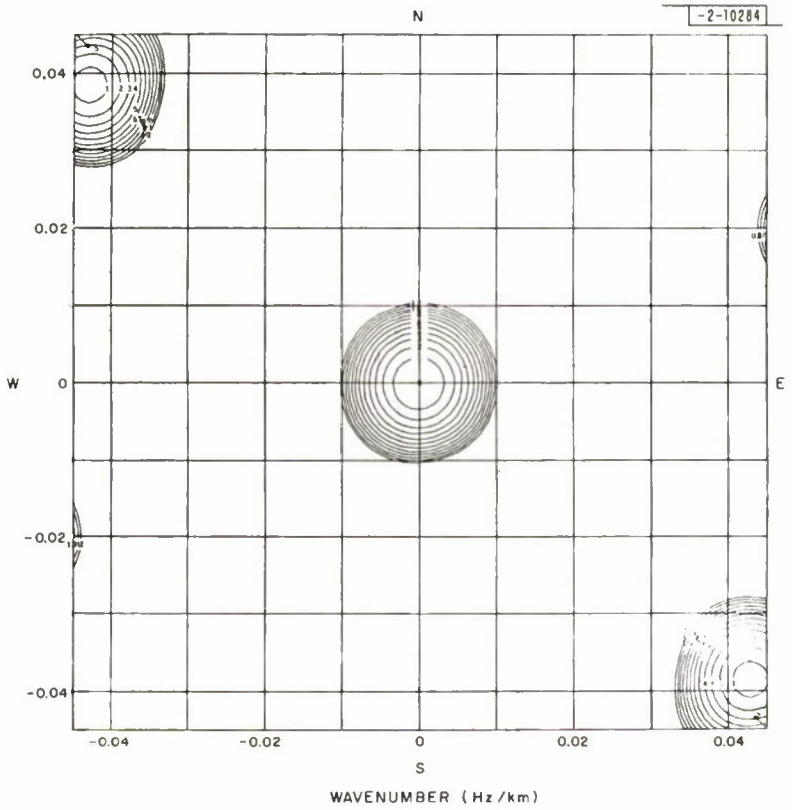

Fig. III-6. Beam pattern for ALPA.

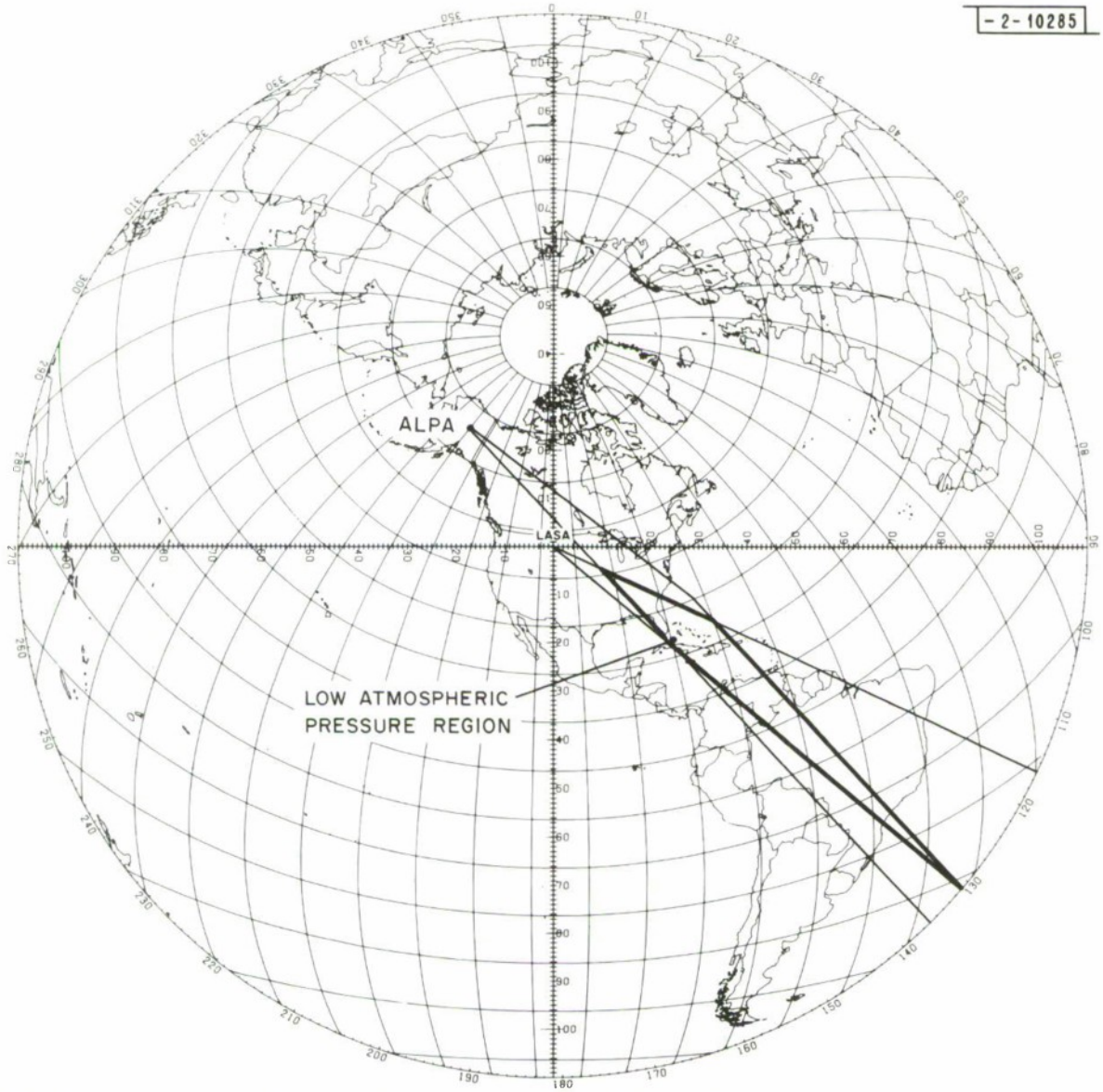

Fig. III-7. Location of 16 September 1970 noise source at 0640 to 0740 using ALPA and LASA simultaneously.

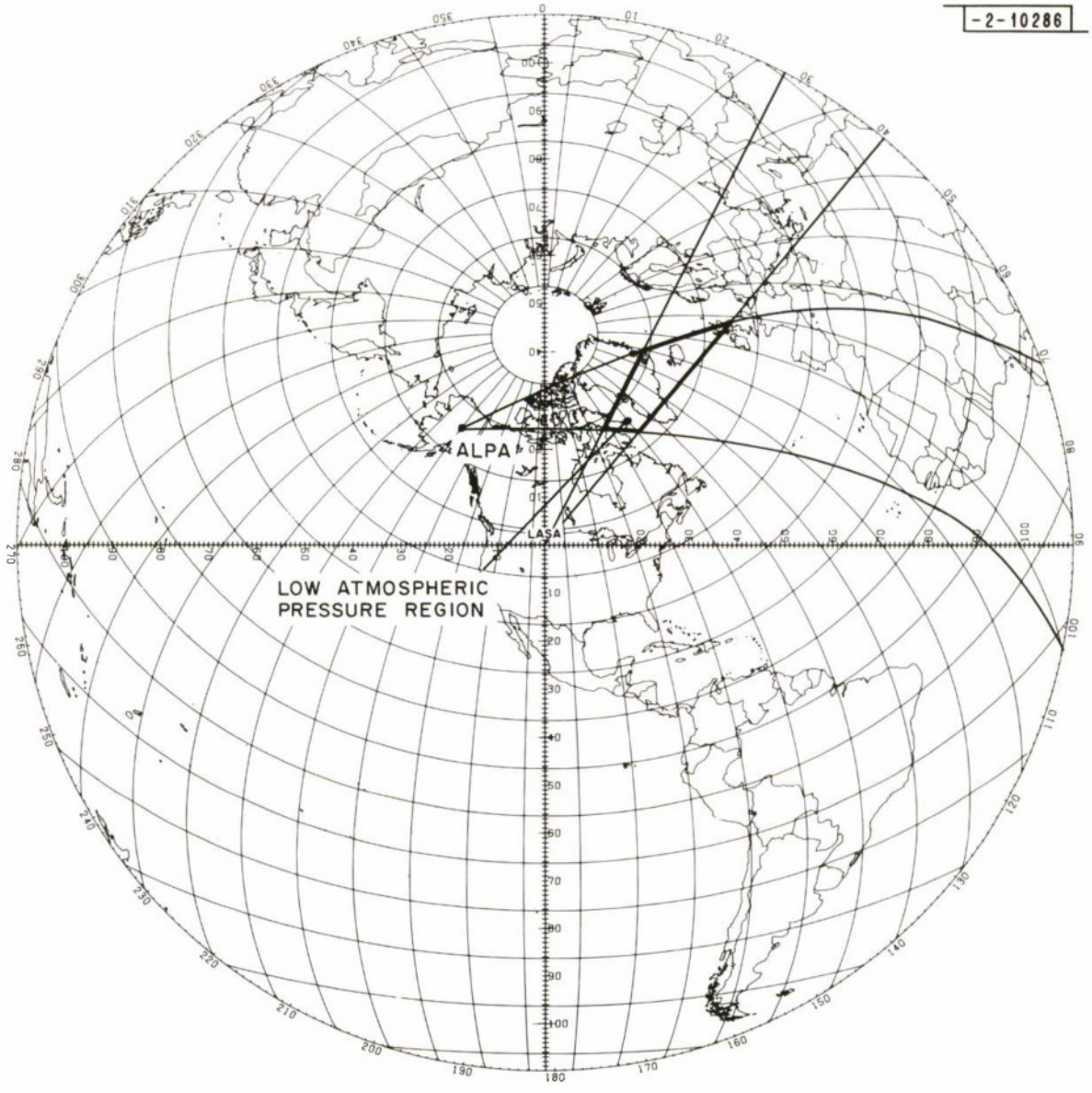

Fig. III-8. Locotion of 20 October 1970 noise source ot 0550 to 0650 using ALPA ond LASA simultoneously.

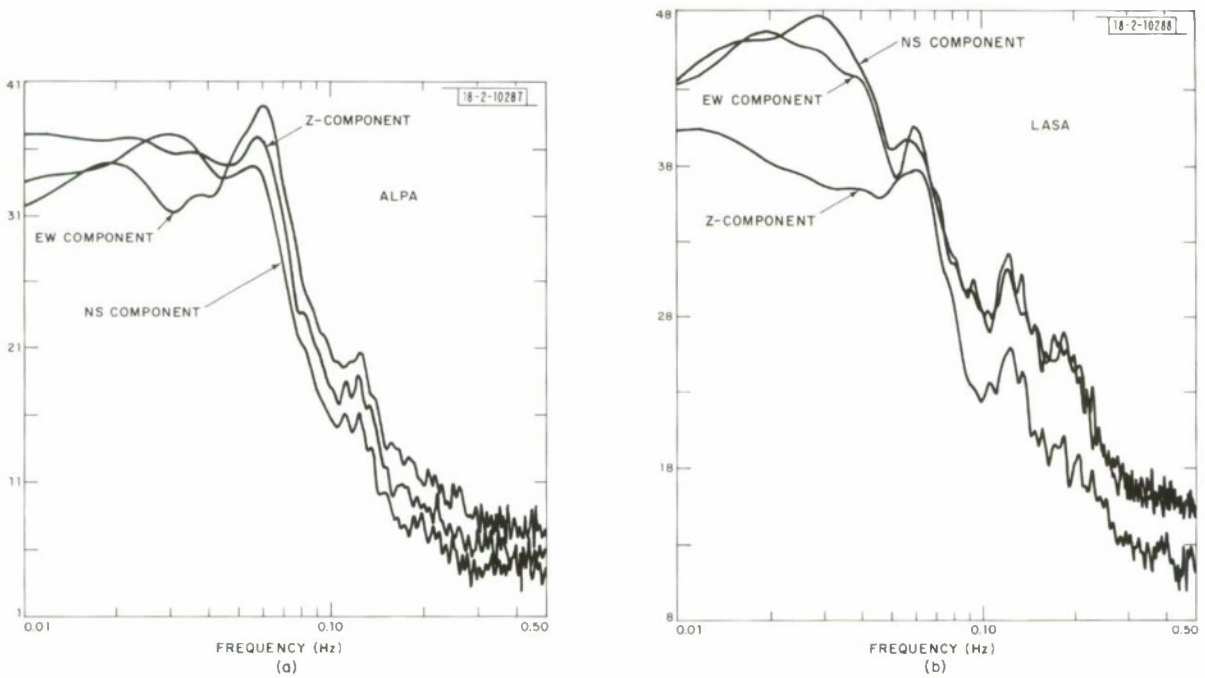

Fig. III-9. Camparison of power spectra of naise at (a) ALPA and (b) LASA from 0640 to 0740 on 16 September 1970. Pawer is measured in decibels relative ta 1 $m\mu^2$/Hz at 0.04 Hz.

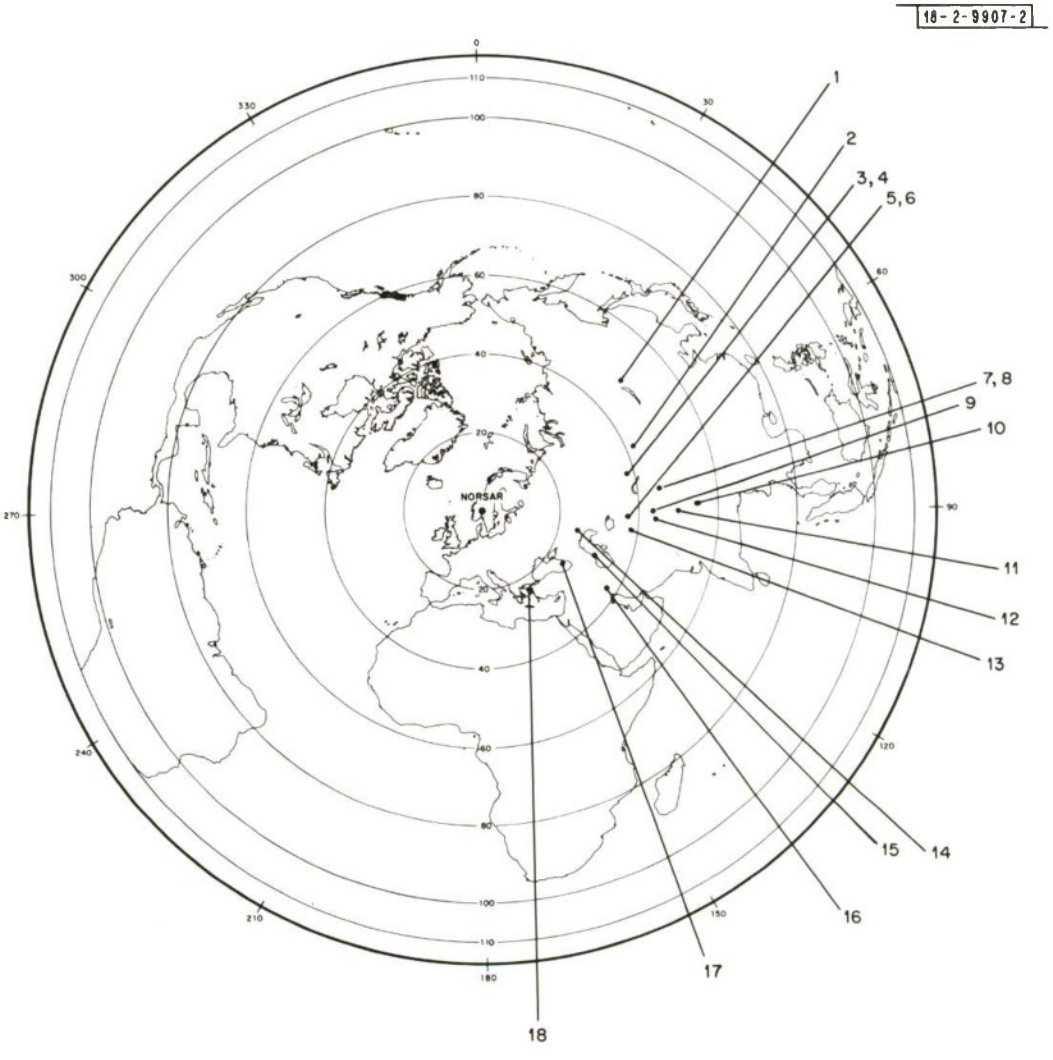

Fig. III-10. Location of events studied relative to NORSAR.

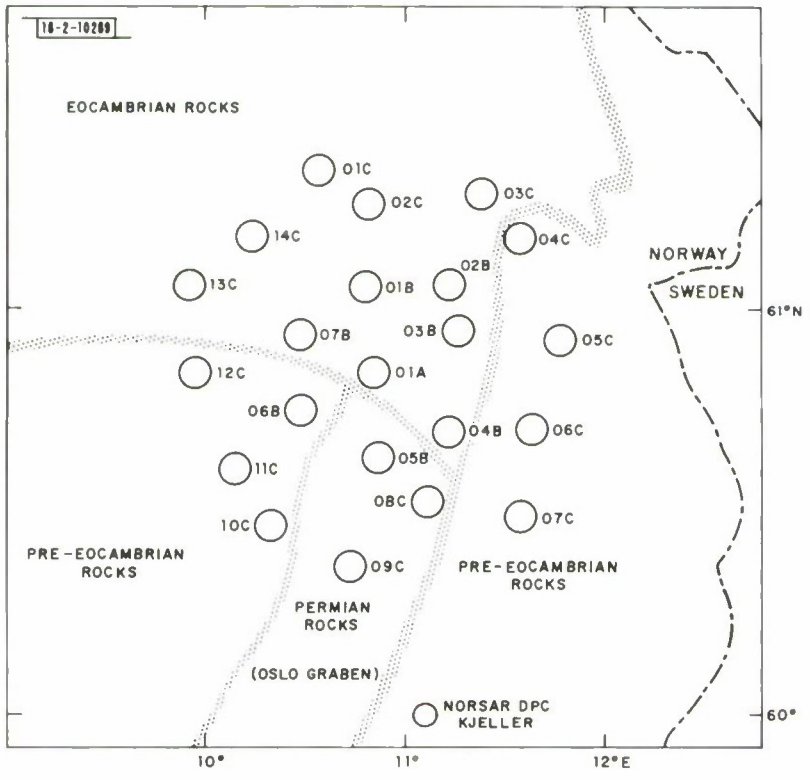

Fig. III-11. NORSAR configuration with outline of geology.

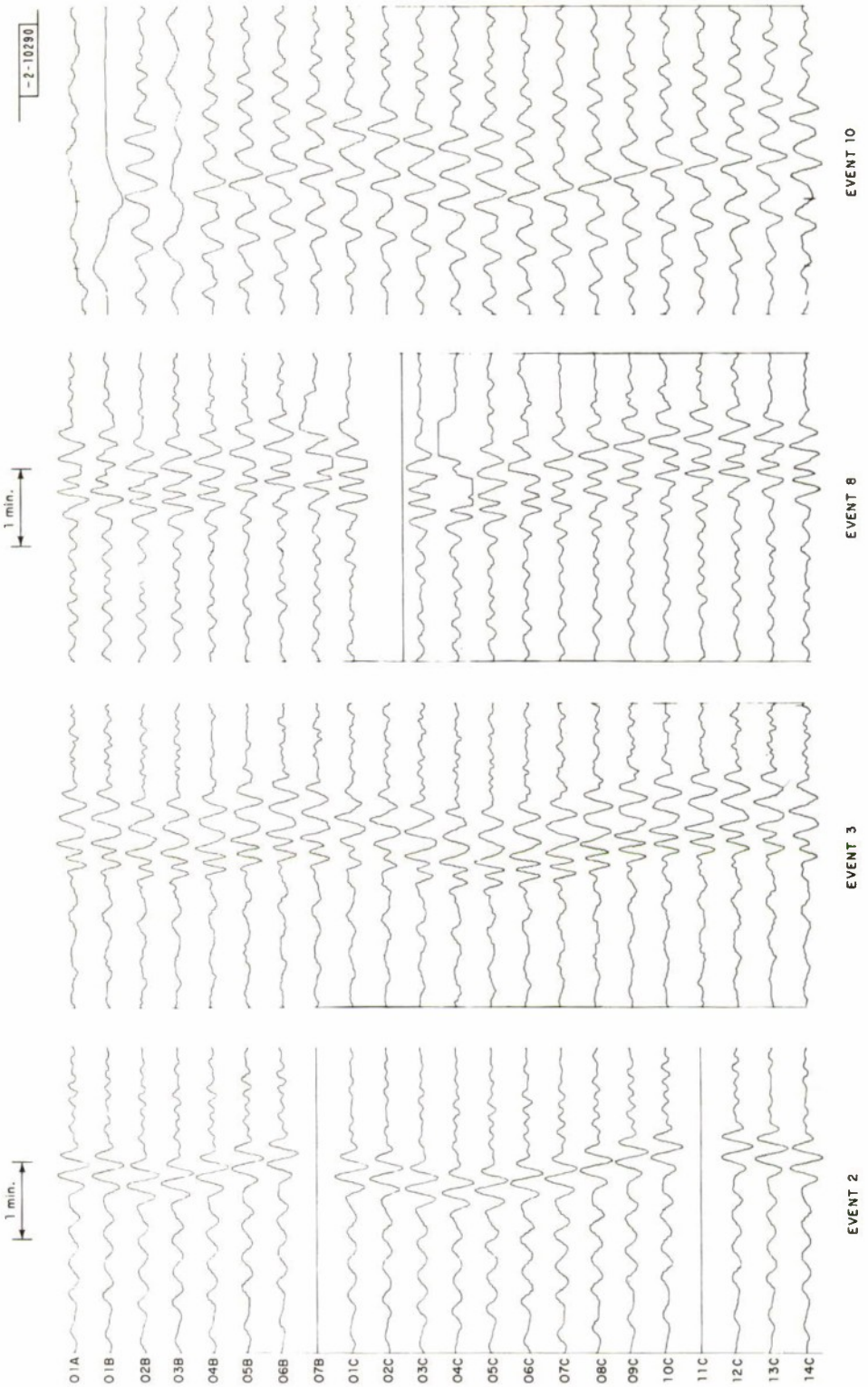

Fig. III-12. NORSAR long-period vertical records for four Asian events. All signals normalized to peak values.

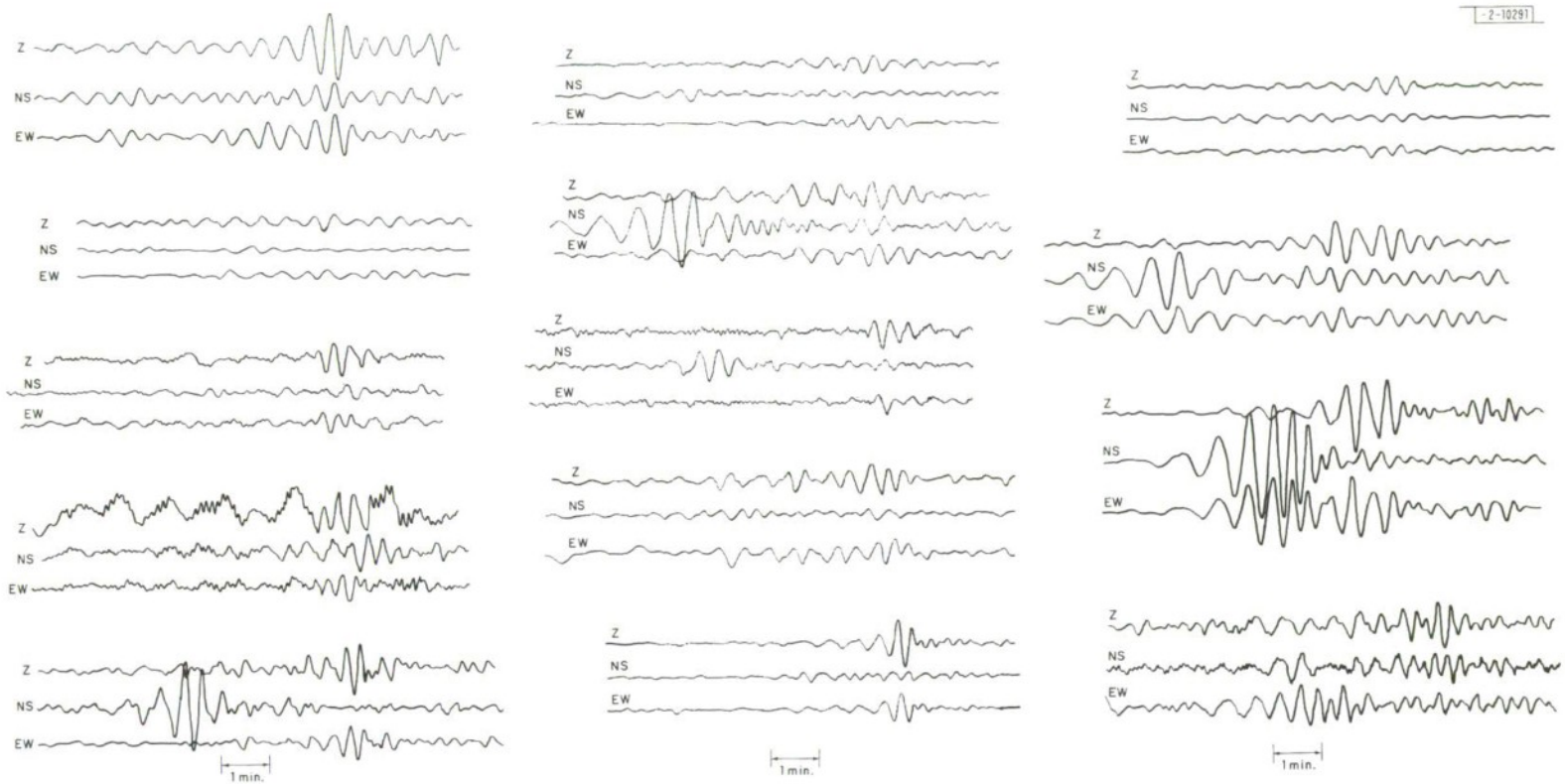

Fig. III-13. Three-component long-period records for fourteen Asian events recorded in Norway.

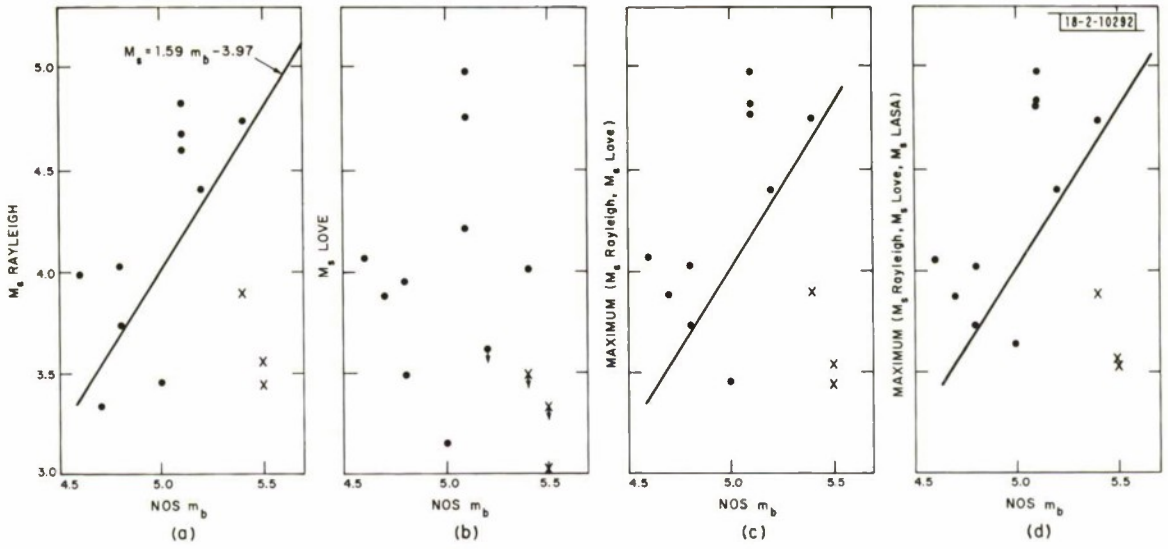

Fig. III-14. M_s-m_b plots using NOS m_b: (a) Narway Rayleigh-wave M_s with period in 18- to 23-sec range; (b) Norway Love-wave M_s far periods greater than 18 sec; (c) larger value from (a) and (b) used for M_s; and (d) larger value fram (c) and LASA M_s used far M_s.

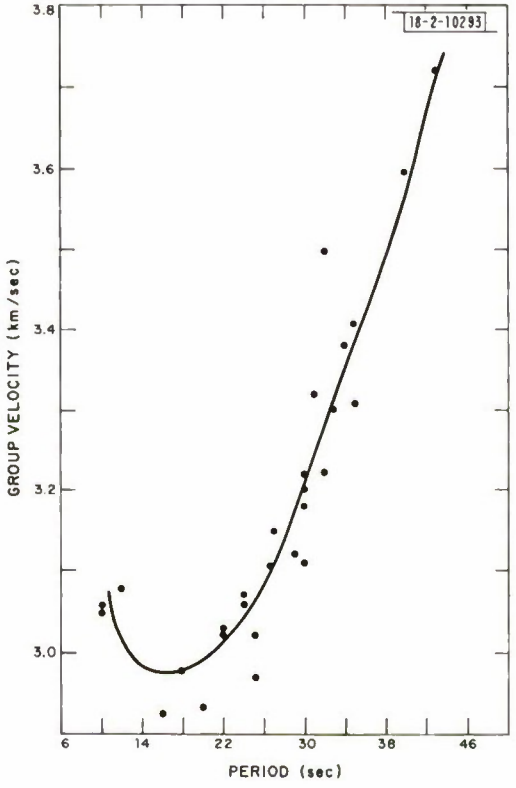

Fig. III-15. Rayleigh-wave graup-velacity meosurements ot NORSAR fram 4 events in central Asia.

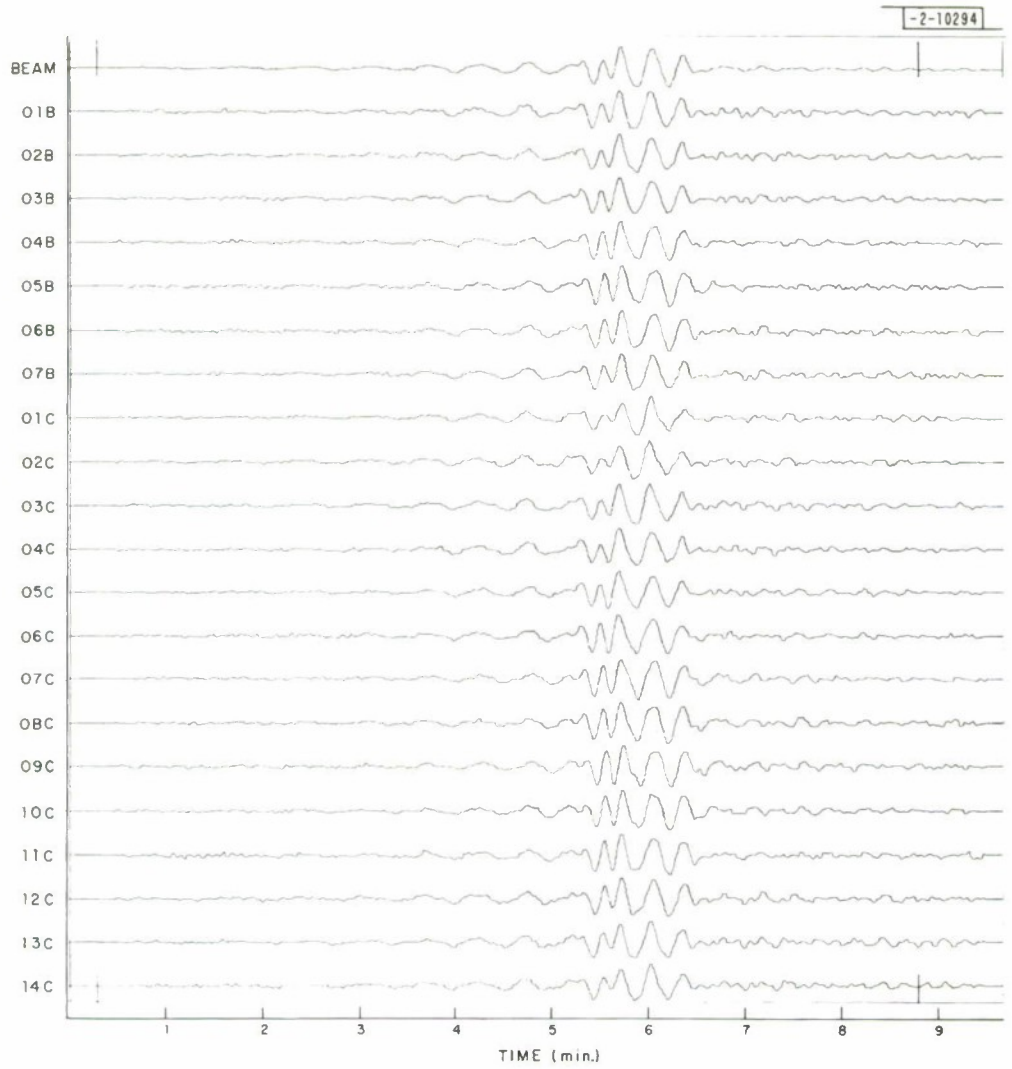

Fig. III-16(a). Beam and aligned traces of Rayleigh waves from Eastern Kazakh event of 25 April 1971.

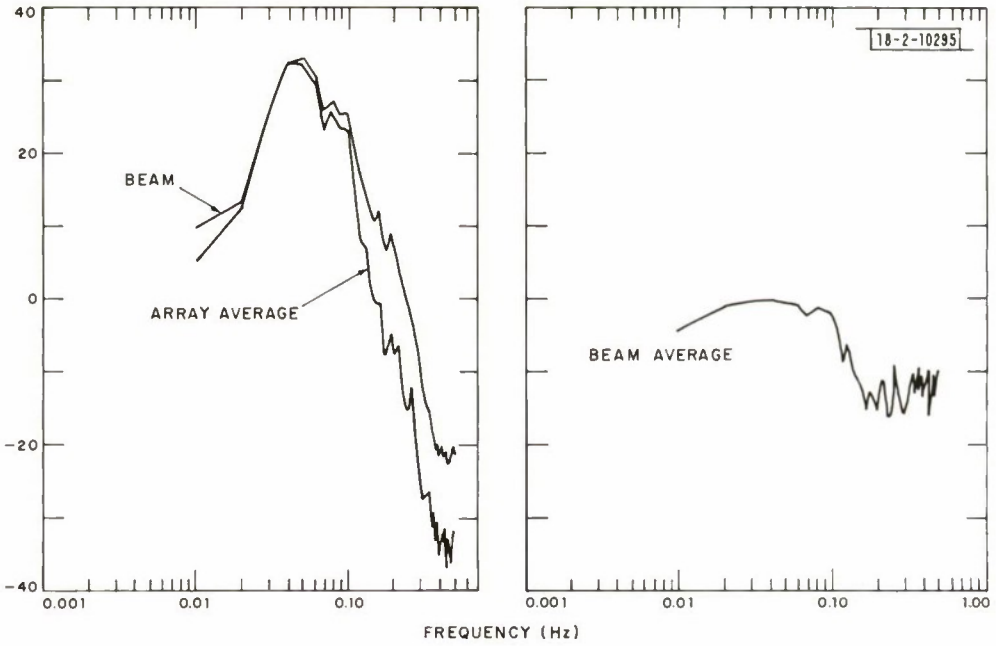

Fig. III-16(b). Power spectrum of beam and array average-power spectrum, and difference between the two. Power is measured relative to 1 $m\mu^2$/Hz at 20 sec.

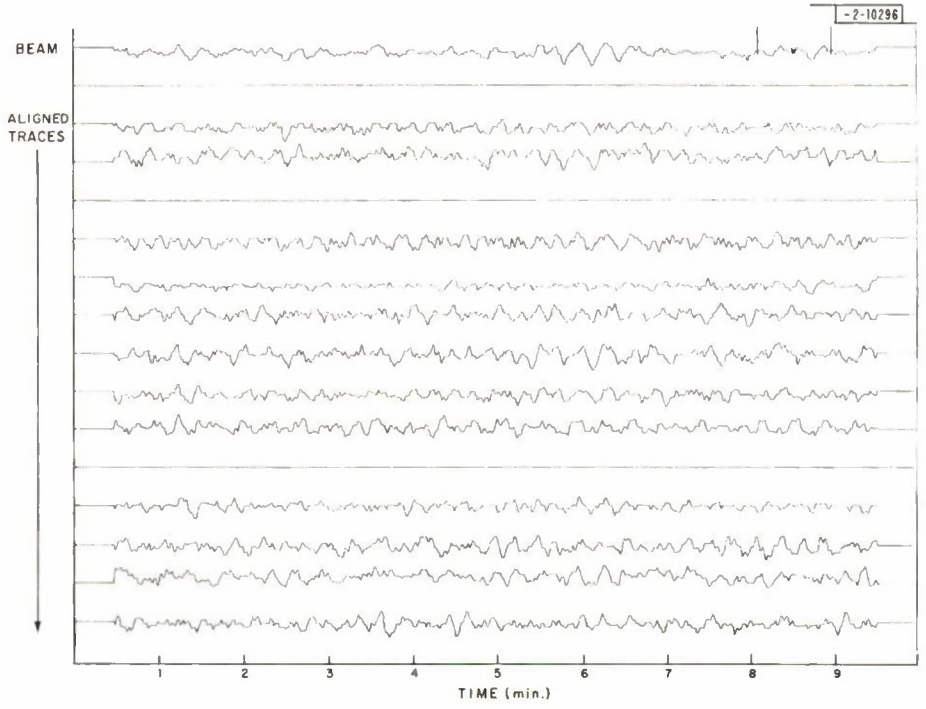

Fig. III-17. Beam and aligned traces of Eastern Kazakh event of 25 May 1971.

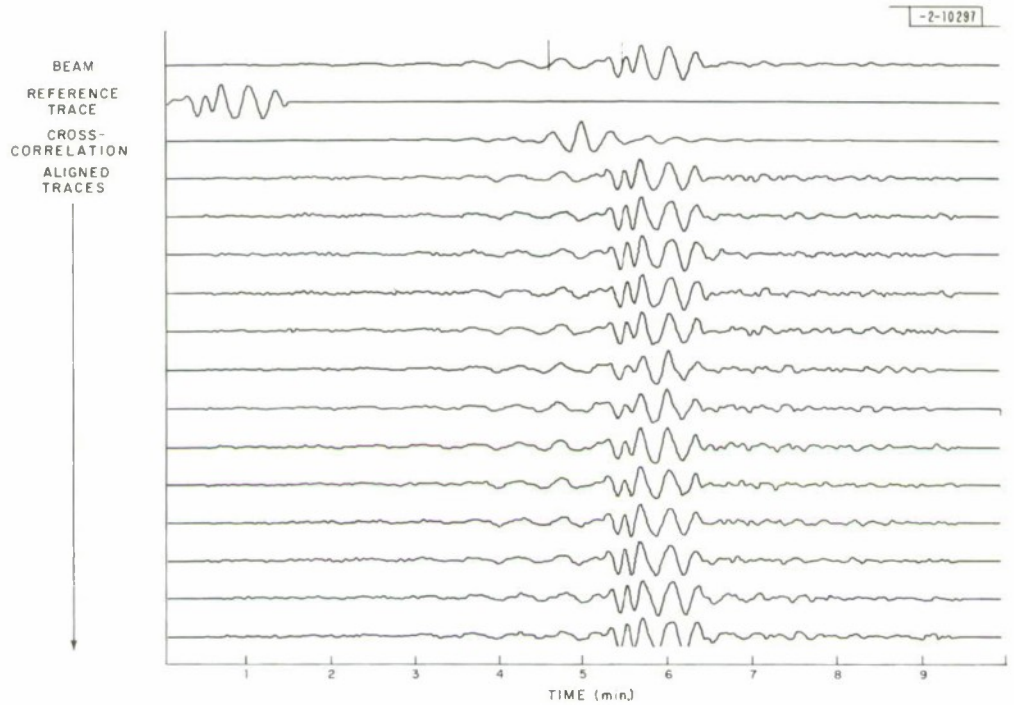

Fig. III-18. Rayleigh-wave beam af event of 25 April 1971; reference waveform fram 90-sec partian af this beam; and cross-correlatian of reference trace and beam.

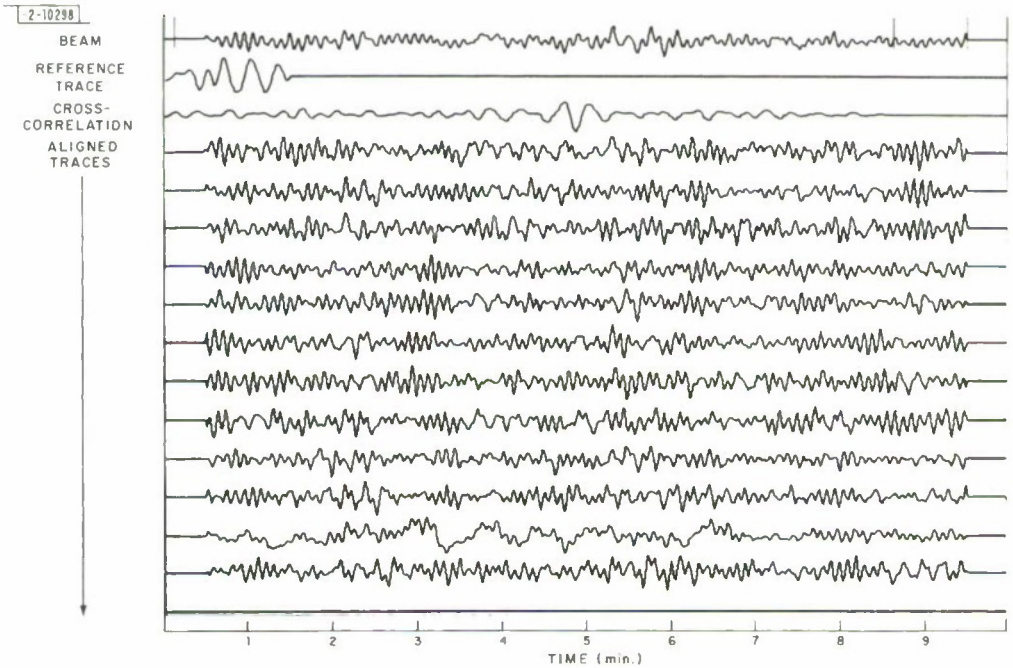

Fig. III-19. Rayleigh-wave beam af event fram Eastern Kazakh an 9 October 1971; reference wavefarm fram event of Fig. III-18; and cross-carrelation af reference trace and beam.

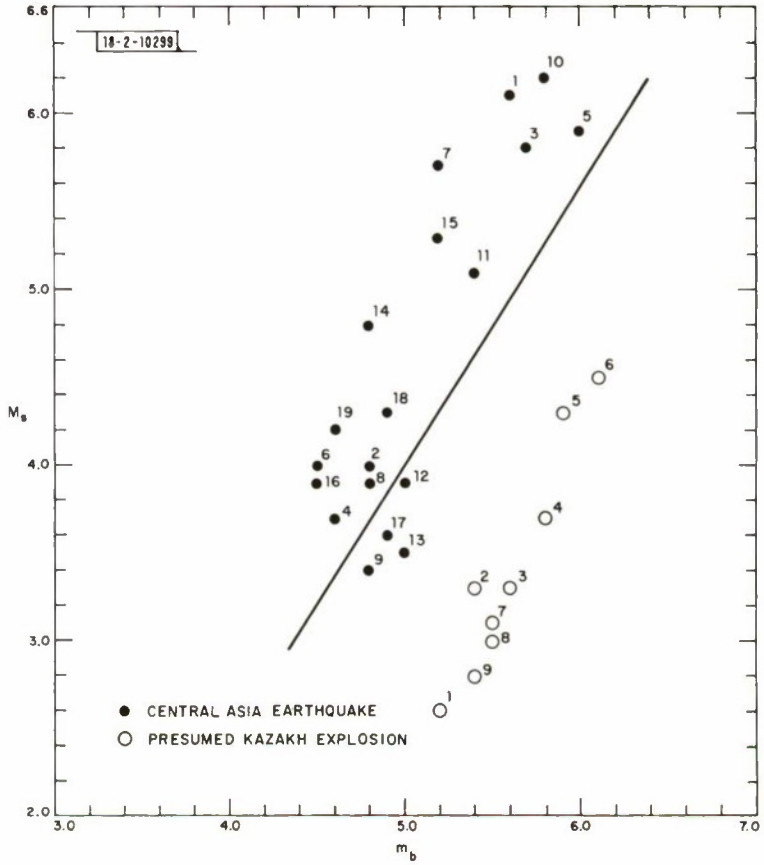

Fig. III-20. M_s-m_b diagram. M_s measured at NORSAR, m_b NOS or SAAC determinatian.

IV. NETWORK CHARACTERISTICS

A. DETECTION AND DISCRIMINATION OF CENTRAL ASIAN EARTHQUAKES AND EXPLOSIONS WITH A CONTINENTAL-SIZE WWSSN NETWORK

A study has been undertaken to determine the characteristics of long-period radiation from Central Asian earthquakes and explosions. Such a study will supplement previous work[1-3] with digital data from NORSAR, ALPA and LPE. At present, the data are based on the visual analysis of World-Wide Standard Seismograph Network (WWSSN) film chips contained in the Special Event Library at Lincoln Laboratory. In addition to determining the detection and discrimination capability of an Eurasian WWSSN network, a further goal of this study is to anticipate methods useful in optimizing large-array data analyses for events in Central Asia.

Here the results to date are reported for data collected from twelve Asian and European WWSSN stations. Each station was selected on the basis of high gain, low noise and/or strategic location. A list of the stations is given in Table IV-1. The current data base is comprised of 21 presumed Asian nuclear explosions and 17 Central Asian earthquakes.

A test of the standard M_s-m_b discriminant was made from the events listed in Table IV-2. Figure IV-1 shows the results. The body-wave magnitude m_b was that given by the National Ocean Survey (NOS) when three or more stations reported. Otherwise, the NOS value was combined with a value determined from our 12-element network. Even when a sufficient number of NOS stations reported, the body-wave magnitude from our near-field network was invariably

TABLE IV-1
STATIONS USED IN CENTRAL ASIAN STUDY

Station Symbol	Station	Latitude	Langitude
CHG	Chiengmai, Thailand	18°47'24"N	98°58'37"E
KBL	Kabul, Afghanistan	35°32'27"N	69°02'35"E
KEV	Keva, Finland	69°45'00"N	27°00'00"E
LAH (NIL, 1970)	Lahare, Pakistan	31°33'00"N	74°20'00"E
MSH	Mashed, Iran	36°18'40"N	59°35'16"E
NDI	New Delhi, India	28°42'00"N	77°13'00"E
NUR	Nurmijarvi, Finland	60°30'30"N	24°39'07"E
SHI	Shiraz, Iran	24°38'40"N	52°31'34"E
SHL	Shillang, India	25°34'00"N	91°53'00"E
POO	Paana, India	18°32'00"N	73°51'00"E
QUE	Quetta, Pakistan	30°11'03"N	66°57'00"E
TAB	Tabriz, Persia	38°04'03"N	46°19'36"E

TABLE IV-2

EVENTS USED IN CENTRAL ASIAN STUDY

Event Symbal	Latitude (°N)	Longitude (°E)	Depth (km)	Locatian	m_b (NOS)	No. af Reporting Statians	Date	Time (GMT)
T1	30.3	94.8	22	Tibet	4.9	6	07/14/68	08:12:40.9
T2	31.7	44.7	30	Tibet	5.3	10	06/14/69	03:28:29.6
T3	30.0	95.0	22	Tibet	4.8	1	07/15/68	05:09:05.9
T4	30.3	94.6	30	Tibet	5.0	5	07/13/68	06:05:54.2
K1	49.8	78.2	0	Eastern Kazakh	6.3	18	01/15/65	05:59:58.4
K2	49.8	78.2	0	Eastern Kazakh	6.0	4	11/16/64	05:59:58.0
K3	44.0	79.2	0	Eastern Kazakh	4.9	8	02/27/64	09:02:19.1
K4	44.0	79.3	30	Eastern Kazakh	4.8	8	07/01/68	19:14:54.7
K5	43.8	54.7	0	Urals SSR	5.8	40	12/06/69	07:02:57.4
K6	50.0	77.8	0	Eastern Kazakh	5.7	30	12/28/69	03:46:58.0
K7	50.0	77.7	0	Eastern Kazakh	5.4	22	05/31/69	05:01:56.6
K8	49.8	78.1	0	Eastern Kazakh	5.5	29	10/30/67	06:03:57.9
K9	49.8	78.1	0	Eastern Kazakh	5.6	15	05/16/64	06:00:57.8
KA	49.8	78.0	0	Eastern Kazakh	5.6	14	03/15/64	07:59:58.2
KB	49.9	78.2	0	Eastern Kazakh	5.5	11	07/19/64	05:59:58.6
KC	49.8	78.1	0	Eastern Kazakh	5.6	17	03/03/65	06:14:56.8
KD	49.8	77.9	0	Eastern Kazakh	5.2	5	05/11/65	06:39:57.3
KE	50.0	78.1	0	Eastern Kazakh	5.4	13	06/17/65	03:44:57.0
KF	49.7	78.2	0	Eastern Kazakh	4.6	2	12/29/69	04:01:58.2

TABLE IV-2 (Continued)

Event Symbal	Latitude (°N)	Longitude (°E)	Depth (km)	Location	m_b (NOS)	No. of Reporting Stations	Date	Time (GMT)
KH	57.7	65.2	33	Central Kazokh	4.7*	15	10/06/67	07:00:02.5
KI	49.7	77.9	0	Eastern Kazakh	4.8	16	05/07/66	03:57:58.2
KJ	49.8	78.2	0	Eastern Kazokh	5.8	31	09/29/68	03:42:57.5
KK	49.9	78.3	0	Eastern Kazokh	5.5	23	07/23/69	02:46:58.09
KL	49.7	78.2	0	Eastern Kazakh	5.3	28	07/04/69	02:46:57.02
C1	53.7	81.4	11	Centrol Russio	5.3	10	02/15/65	12:34:55.1
C2	21.6	111.9	33	Eastern China	5.4	16	07/25/69	22:49:41.28
C3	38.1	119.4	32	Northeast China	5.0	10	07/18/69	13:33:48.37
S1	43.1	94.5	33	Sinkiang	5.3	3	10/26/64	15:16:48.2
S2	41.7	82.3	30	Sauthern Sinkiang	5.0	11	04/27/67	23:15:19.7
S3	42.6	84.6	0	Sinkiang	4.9	6	06/05/64	02:36:15.2
S5	41.6	75.1	30	Kirgiz	4.8	1	12/08/68	15:51:59.9
S6	41.4	79.2	30	Kirgiz-Sinkiang	5.8	18	02/11/69	22:08:54.7
S7	39.8	77.8	33	Southern Sinkiang	5.0	6	07/20/69	04:34:14.9
S8	41.1	75.8	39	Kirgiz SSR	5.1	4	06/29/69	03:40:12.95
M1	51.9	98.9	26	USSR Mangolia	4.9	18	05/10/66	21:04:08.1
N1	73.4	53.9	0	Novoya Zemlya	4.9	9	10/25/64	07:59:58.3
N2	73.2	54.4	0	Novoya Zemlyo	4.3	5	09/18/64	07:59:54.8
R1	40.1	70.7	30	Tadzhik SSR	5.0	2	12/09/69	13:41:09.0

* ISC Bulletin.

within one-half a magnitude unit. The surface-wave magnitude M_s was computed by measuring the peak-to-peak amplitude A (in microns) and the corresponding period T (in seconds) of the Rayleigh wave at its maximum and applying[4]:

$$M_s = \log(A/T) + 0.92 + \log(\Delta) \qquad \Delta < 25°$$

$$M_s = \log(A/T) + 1.66 \log(\Delta) \qquad \Delta \geq 25°$$

Maximum values were read to maintain maximum detectability.

For a given event, the plotted M_s value was averaged over the values determined at the various detecting stations. Typical single-event scatter of M_s is presented in Fig. IV-2. When a surface wave was not detected, the amplitude of the noise in the signal band was measured. In these cases, an upper limit on the surface-wave magnitude was computed by assuming detectability of a waveform when the signal-to-noise ratio was one-to-one. Data points computed in such a manner are marked with an arrow. The tail of the arrow marks the average of the four lowest values, while the head of the arrow points to the single lowest value.

Observations based on the M_s-m_b measurements are:

(1) The surface waves from all events with $M_s \geq 3.5$ are detected. It seems probable that the inclusion of more data will lower that figure to $M_s \geq 3.1$. Further, a factor-of-four improvement in signal detectability would lower the value to 2.9 and possibly down to 2.4. It seems reasonable that digitization of the network would give such an improvement.

(2) The events clearly separate into two populations. However, any linear relationship between M_s and m_b that extends below $m_b = 5.0$ will have large scatter. The most troublesome events at $m_b = 5.0$, $M_s = 3.5$ are geographically confined to a small area in Tibet.

The separation between natural and artificial M_s-m_b values has been shown to improve by measuring magnitudes at longer periods.[2,3] Since we used maximum Rayleigh-wave amplitudes, the poor separation at low magnitudes shown in Fig. IV-1 might be improvable. Two of the natural events in our data base contained sufficient broadband energy to make an estimate of the decay of M_s with increasing period. A plot of the results in Fig. IV-3 indicates that a drop of at least one unit of surface-wave magnitude can be expected between 12 and 30 sec. Such a decrease is consistent with North American explosion data.[2] Even though our data are quite limited, the supposition of a much improved M_s-m_b discriminant, based on longer period measurements, seems tenuous.

Of particular interest to NORSAR capabilities are the characteristics of waves observed at the Finland stations, Kevo and Nurmijarvi. As shown in Fig. IV-2, at least one of the stations has the maximum M_s recorded by the array in 6 out of the 8 events, often by half a unit of surface-wave magnitude. In the 15 events in the complete data base in which at least one of the stations made an observation, one or both was a maximum or well above average 13 times. The average period of the arrivals was 12 to 14 sec. It seems clear that the continental path from Mid-Asia to Scandinavia is an efficient one for short-period surface waves over teleseismic distances. Since it is not uncommon to have relatively low noise in the 10- to 15-sec band, NORSAR surface-wave detection capabilities may be aided by examining data in that period range. It has been noticed that NORSAR M_s values based on 20-sec Rayleigh-wave data from Central Asia are anomalously low.[5]

In the future, NORSAR, ALPA and LPE data will be included in our analysis and the combined capabilities of these arrays with WWSSN will be used in determining the source and path characteristics for Eurasian events.

T. E. Landers

B. SHORT-PERIOD NETWORK CAPABILITY

In conjunction with the experiment mentioned in the previous section, we are investigating issues connected with the production of a more adequate low-magnitude bulletin. One such issue is the detection level and credibility of the LASA detection processor; another is the detection level of the WWSSN stations for events in the Sino-Soviet area.

The experiment is being done in two phases. The first phase is to determine the world seismic activity for a given period – in this case, January 1970. The second phase will then be to see if the long-period waves from the events can be detected on the worldwide network. An important aspect of this experiment is to set it up in such a way that the procedures used may be suitable for the routine processing of any or all periods in the future.

In an effort to compile as complete a list of epicenters as possible for this study, the National Ocean Survey recomputed all their data for January 1970. The more than 700 events they were able to locate will form one of the main data sources. For this same month, the LASA detection log indicated more than 2000 possible event detections. The input from these two sets of data will form the main starting point for the effort to produce as complete a list of epicenters as possible. Since many of the events in the initial list will be phases or false alarms, it will be necessary to investigate each entry individually. Those events that are phases can usually be eliminated in the first step. When this is done, the NOS list will yield epicenters with a high degree of reliability. However, the LASA detection log is left with a large number of detections that must be individually investigated. An example of this is an event which appeared on the LASA bulletin as an unlocated event arriving from the east. This event recorded best on a beam centered at 37° N 26° E and triggered an additional 38 beams. By using the location of the beam as the epicenter, arrival times were computed to some of the near WWSSN stations. This event could later be seen on ATU (Athens University, Greece) and EIL (Eilat, Israel) as shown in Fig. IV-4. The epicenter was located at 37.2° N 28.1° E, and had a magnitude less than 4.0. Each LASA detection log event is being studied in this way. Early results indicate we can expect that 50 or 60 events per day will be verified in this way. The addition of a detection log from any other large array, such as NORSAR, may double this number.

R. E. Needham
R. M. Sheppard

REFERENCES

1. P. D. Marshall and P. W. Basham, "Discrimination between Earthquakes and Underground Explosions Employing an Improved M_s Scale," Geophys. J. (in press).
2. J. F. Evernden, W. J. Best, P. W. Pomeroy, T. V. McEvilly, J. M. Savino and L. R. Sykes, "Discrimination between Small-Magnitude Earthquakes and Explosions," J. Geophys. Res. 76, 8042-8055 (1971).
3. J. Savino, L. R. Sykes, R. C. Liebermann and P. Molnar, "Excitation of Seismic Surface Waves with Periods of 15 to 70 Seconds for Earthquakes and Underground Explosions," J. Geophys. Res. 76, 8003-8020 (1971).
4. J. F. Evernden, "Variation of Rayleigh-Wave Amplitude with Distance," Bull. Seismol. Soc. Am. 61, 231-240 (1971).
5. J. Filson, private communication.

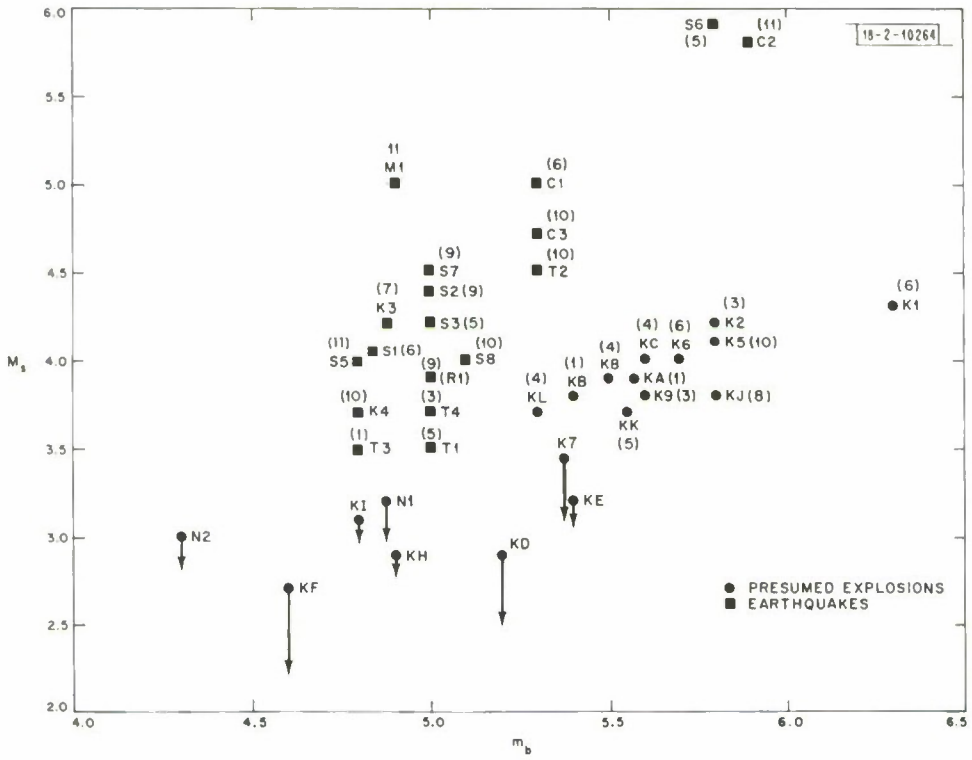

Fig. IV-1. M_s-m_b relationship for Asian earthquakes and explosions. Arrows indicate that an upper-limit estimate based on signal band noise was made. Maximum Rayleigh-wave amplitudes were used. Letter symbols identify events; number of recording stations for each event is indicated by numerals in parentheses.

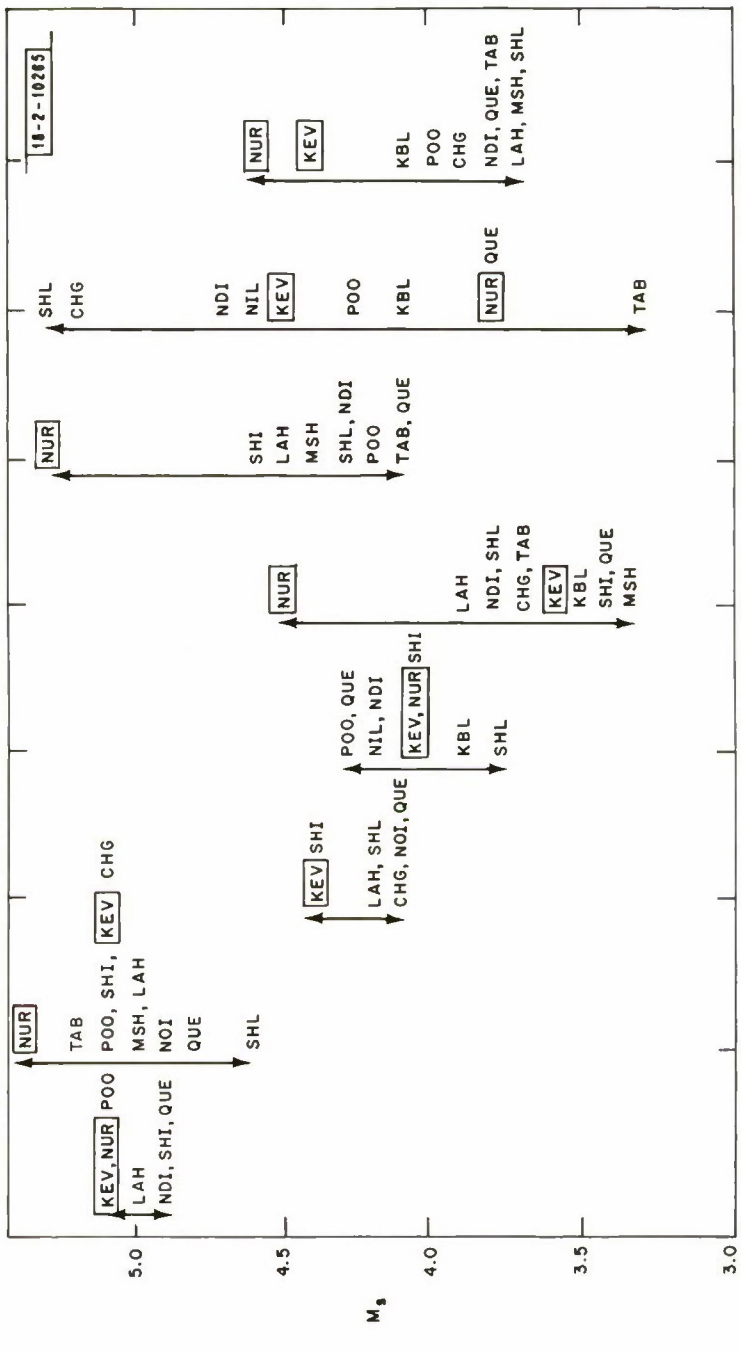

Fig. IV-2. Single-event M_s scatter. Event symbols refer to Table IV-2. Note behavior of Finland Stations, Nurmijarvi and Kevo.

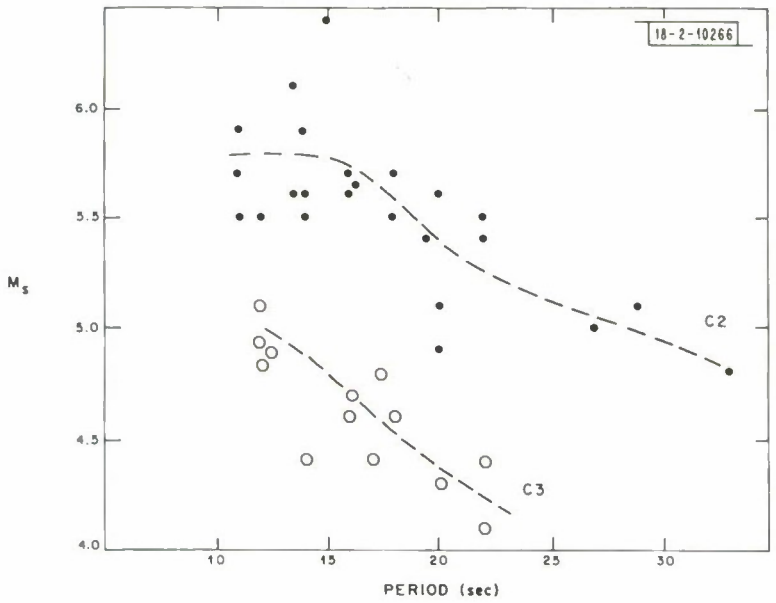

Fig. IV-3. Behaviar af M_S as a functian af periad far twa Asian earthquakes. Event symbals refer ta Table IV-2.

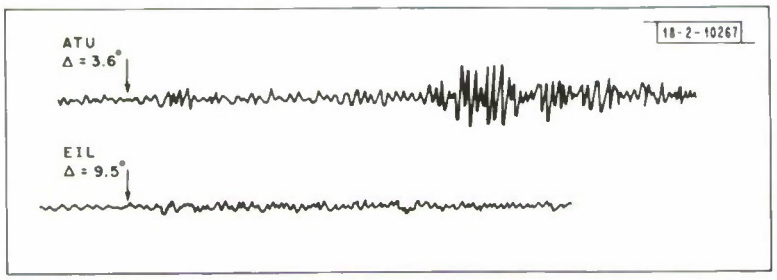

Fig. IV-4. Verification of a LASA beam detectian on shart-period seismameters at Athens and Eilat.

V. LONG-PERIOD SEISMOMETERS

A. NONPROPAGATING NOISE IN LONG-PERIOD SEISMOMETERS

It has been known for some time that the noise measured by long-period seismometers is composed of two parts: propagating noise which is coherent over distances of at least 100 km, and nonpropagating noise which is incoherent over distances greater than a few kilometers. The nonpropagating component is therefore completely uncorrelated between long-period instruments at LASA and can only be reduced by $\sqrt{n}$ by summing n instruments. However, Capon[1] has shown using coherence spectra that there is a significant correlation between measured long-period seismic noise and microbarograph recordings at the same site at times when the nonpropagating component is appreciable. Since this component contributes at least 40 percent of the noise up to 50 percent of the time,[1] it seemed worthwhile to consider the possibility of eliminating this noise using the fact that it is correlated with the output of the nearby microbarograph.

We can divide the seismometer output S(t) into two parts: that which is correlated with the microbarograph output, and therefore caused by local atmospheric pressure fluctuations N(t); and that part not correlated with the microbarograph output E(t). Thus,

$$S(t) = N(t) + E(t) \quad . \tag{V-1}$$

It is possible to define an atmospheric pressure fluctuation in the vicinity of the seismometer and microbarograph which would produce a unit positive impulse in the output of the microbarograph, and some other response I(t) in the output of the seismometer. In this case, if the microbarograph output is M(t), the pressure-induced noise N(t) in the seismometer output is given by

$$N(t) = \int_{-\infty}^{\infty} M(\tau)\, I(t - \tau)\, d\tau \quad . \tag{V-2}$$

If we define the cross-correlation function to be

$$\varphi_{AB}(\ell) = \int_{-\infty}^{\infty} A(t + \ell)\, B(t)\, dt \tag{V-3}$$

it can be shown that

$$\varphi_{SM}(\tau) = \int_{-\infty}^{\infty} I(s + \tau)\, \varphi_{MM}(s)\, ds \tag{V-4}$$

where we have used the knowledge that E(t) and M(t) are uncorrelated (by definition) or, mathematically,

$$\varphi_{EM}(\tau) = 0 \qquad \text{for all } \tau \quad . \tag{V-5}$$

Equation (V-4) can be solved for I(t), which can be convolved with the microbarograph output to obtain an estimate of the pressure-induced noise [Eq. (V-2)]. This predicted noise can be subtracted from the seismic signal S(t) to reduce the noise level.

This method was applied to a noise sample from the 3-component instrument at A0 at LASA, beginning 17h 20m 00s on 23 August 1967. Capon[1] showed that the nonpropagating component

contributed nearly 10 dB more to the noise measured by the vertical component than did the propagating part. Figure V-1 shows the microbarograph output (1), the seismometer output (2) the predicted noise (3), and the seismometer output with the predicted noise subtracted (4) for each of the three components (a) vertical, (b) north-south, and (c) east-west. In Fig. V-2 can be seen the coherence spectra between the microbarograph and the seismometer (1), and between the microbarograph and the seismometer output with the predicted noise subtracted (2) for (a) vertical, (b) north-south, and (c) east-west components. The big reduction in coherence in the seismic signal bandwidth from Fig. V-2(1) to 2(2) for each component indicates that much of the pressure-induced noise has been eliminated. It is therefore possible to reduce this kind of noise significantly at every site at which there is also a microbarograph.

This work does not indicate how much of the pressure-induced noise is due to buoyancy effects in the seismometer, or how much is the result of ground displacements caused by fluctuations in atmospheric pressure. The atmospherically produced ground displacement is a spatial integration of the whole pressure pattern around the seismometer; the fluctuations in ground displacement depend on the variation of the pressure pattern with time.[2] We would therefore expect the stability of the function I(t) to depend on the weather if the ground-loading effect were dominant. On the other hand, if the buoyancy effect were dominant, we would expect I(t) to be as stable as the responses of the microbarograph and seismometer.

To determine which of these effects is the more important, the previously computed transfer functions I(t) for each seismometer component at A0 were applied to a noise sample beginning 19h 50m 00s on 1 July 1967, which Capon[1] found to have a large nonpropagating component. The microbarograph output (1), the seismometer output (2), the predicted noise [using the I(t) calculated from the 23 August sample] (3), and the difference between the seismometer output and the predicted noise (4) are shown for each component of the seismometer at A0 in Fig. V-3. The predicted noise appears to bear little relation to the measured noise, and on subtraction from it even increases the noise amplitude. We may conclude from this and the foregoing argument that the ground-loading effect is dominant.

Herrin, et al.[3] have reported coherencies between noise measured by long-period seismometers and microbarographs at Grand Saline, Texas. They were particularly careful to isolate the seismometers from buoyancy effects, and their results clearly show that the measured noise exhibited the qualities which would be expected from Sneddon's theoretical considerations[2]: the decay of amplitude with depth of seismometer emplacement, and the dependence on the way in which the surrounding pressure pattern varies.

Since the ground-loading effect has a critical spatial as well as time dependence, the noise measured by a seismometer could be predicted with some confidence only from an array of microbarographs all situated within a radius of a few kilometers of the seismometer.

A. M. Ziolkowski

B. DISCUSSION OF DATA FROM THE IGPP QUARTZ ACCELEROMETER

Long-period digital data from a new wideband accelerometer[4] have been supplied to us by Professor B. Block of IGPP, University of California, San Diego. The instrument was located at a surface site (vault at a depth of 10 feet) near the coast on the boundary of a Naval Air Base

in California (32.88°N, 117.1°W). The output of primary interest to us had a response curve roughly matched to that of instruments used by Pomeroy, et al.[5] The shape of the response is shown, along with the LP LASA response and the WWSSN response, in Fig. V-4. Henceforth, reference to the IGPP instrument will mean the output achieved through the filters which achieve this response curve.

Figure V-5(b) shows the results of noise spectra obtained from the IGPP instrument during April and May 1971. No correction for instrument response has been made. About 90 percent of the observations lie within the dashed lines. We would guess that the height of the peaks at 0.06 and 0.12 Hz would be larger and the entire noise level raised during late fall and winter months, but such data are not available. Figure V-5(a) shows the spectra of Rayleigh waves for two events that are typical of many which have been measured. From these spectra, we note that the best signal-to-noise ratio exists in the 0.03- to 0.05-Hz band. This agrees with results obtained using several narrowband filters at IGPP[6] and at Lincoln Laboratory.

We recognize that sites with less noise at frequencies in the range 0.03 to 0.02 Hz can be found, which will increase the signal-to-noise ratio at those longer periods. However, data in the literature[7] indicate to us that detection capability for earthquakes will not be better at the longer periods at those sites and it will be worse for explosions. Also, good continental paths can exhibit a strong phase with periods as short as 10 sec (see Sec. IV-A). Such a phase may occasionally achieve higher signal-to-noise ratios than in the 0.03 to 0.02 band, but that should normally be the exception.

Instruments with capabilities similar to the IGPP instrument have often been favorably compared with WWSSN instruments for detection purposes, and it is often assumed this is because the newer instruments are not subject to atmospheric buoyancy near 40-sec periods.[7] This is probably partly correct but it is interesting to consider what would happen if the IGPP instrument output were viewed through a noiseless filter designed to give the same frequency characteristics as a WWSSN station. From Fig. V-4 we see that at 8 sec the IGPP instrument is down almost 30 dB relative to the WWSSN. Assuming the noise spectra of Fig. V-5(b) represent ground motion and not buoyancy, we conclude that if the IGPP instrument were corrected to the WWSSN response, the noise at 8 sec would be about 20 dB above the noise at 40 sec, and 10 to 15 dB above the noise at 20 to 25 sec. A signal received under those conditions would require a very strong signal-to-noise ratio in the 20- to 40-sec band to be detected on a trace adjusted so that the 8-sec microseisms would not be too large.

Figure V-6(a-b) graphically demonstrates the situation. A signal from Greece was recorded by the IGPP instrument with a good signal-to-noise ratio. A high-pass filter was applied to reduce the 25-sec signal by about 23 dB and not affect the 8-sec noise. Roughly, this gives a trace with about the same relative amounts of power at 8 and 25 sec which would be seen with a WWSSN response curve. The filtered signal is barely visible and we can see why a WWSSN record would show poor detection capability even if the instruments were not influenced by buoyancy.

This suggests that WWSSN station detection capability could be significantly enhanced by using digital recordings with large dynamic range to allow subsequent filtering, or by directly generating filtered records with the 8- and 16-sec microseisms considerably attenuated. Of course, if buoyancy effects at 20- to 30-sec periods are too large, the gain would not be as

large as indicated by the above demonstration. We believe that relatively modest isolation from atmospheric pressure would be sufficient most of the time. This statement is based upon a consideration of LASA data obtained from instruments with limited pressure isolation. Although there apparently are days when LASA may be significantly influenced by buoyancy in the 20- to 40-sec range, it typically constitutes no more than about half of the recorded amplitude, and even some of that must be due to tilt which is ground motion and cannot be removed in any simple way (see Sec. A above, and also Ref. 1). Also, atmospheric problems are more severe in the 30- to 40-sec band than in the 20- to 30-sec band. Fall and winter days with large microseisms would probably be even less favorable to the WWSSN recordings.

We cannot fairly discuss the situation which would obtain at a site very quiet at 40 sec where the buoyancy problem would be more severe except for instruments such as the IGPP accelerometer or standard instruments extremely isolated from the environment, such as the Lamont LPE installations.

R. T. Lacoss
E. N. Ashley, Jr.

REFERENCES

1. J. Capon, "Investigation of Long-Period Noise at the Large Aperture Seismic Array," J. Geophys. Res. 74, 3182-3194 (1969), DDC AD-671509.
2. I. A. Sneddon, "The Stress Produced by a Pulse of Pressure Moving Along the Surface of a Semi-Infinite Solid," Rendiconti Circolo Matimatico di Palermo 2, 57-62 (1952).
3. E. T. Herrin, G. G. Sorrells and J. A. McDonald, "A Digital Acquisition System for Geophysical Data and Some Preliminary Results," in Copies of Papers Presented at Woods Hole Conference on Seismic Discrimination, Vol. 1 (1970).
4. B. Block and R. D. Moore, "Tidal to Seismic Frequency Investigations with a Quartz Accelerometer of New Geometry," J. Geophys. Res. 75, 1493-1505 (1970).
5. P. W. Pomeroy, G. Hade, J. Savino and R. Chander, "Preliminary Results from High Gain Wide-Band Long-Period Electromagnetic Seismograph Systems," J. Geophys. Res. 74, 3295-3298 (1967).
6. B. Block and J. Dratler, private communication.
7. J. Savino, L. R. Sykes, R. C. Liebermann and P. Molnar, "Excitation of Seismic Surface Waves with Periods of 15 to 70 Seconds for Earthquakes and Underground Explosions," J. Geophys. Res. 76, 8003-8020 (1971).

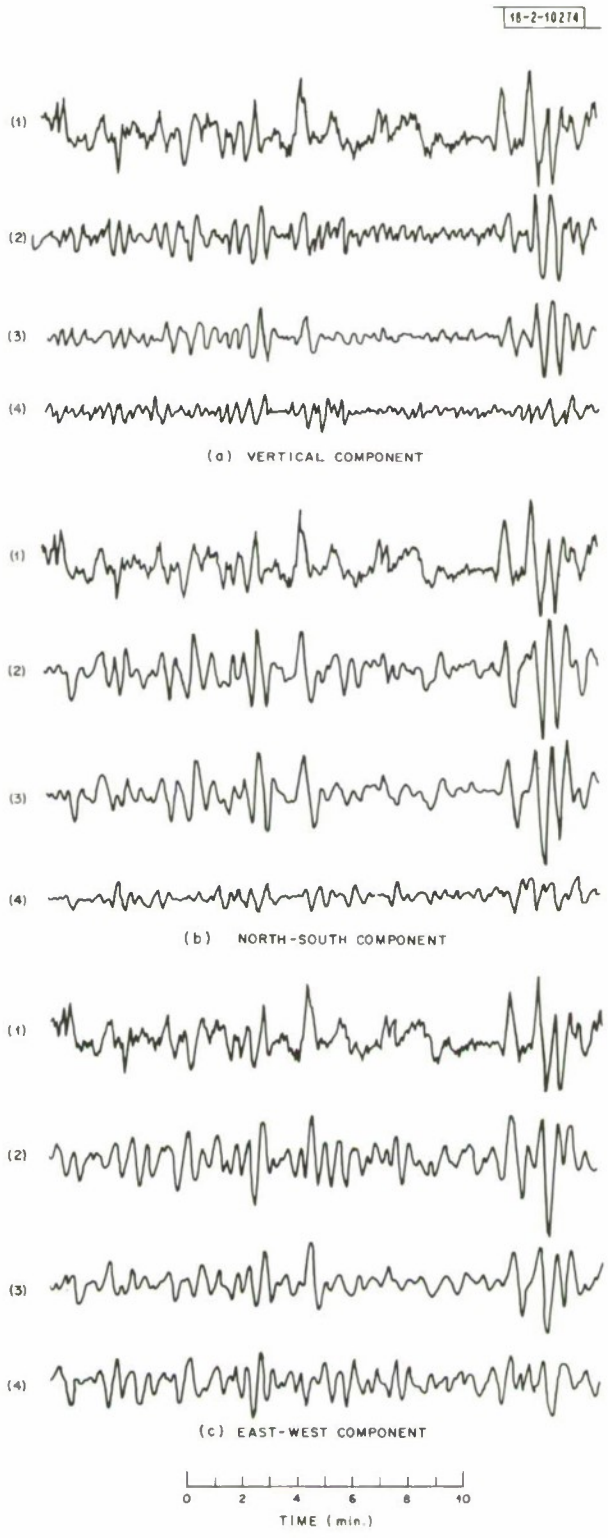

Fig. V-1. Data from LASA site A0 beginning 17h 20m 00s an 23 August 1967. Far each af three components of seismameter (a) vertical, (b) narth-south, and (c) east-west are shawn seismameter autput (2), predicted noise in that autput (3), and seismameter autput minus predicted naise (4). In each case, (1) is microbarograph autput at A0.

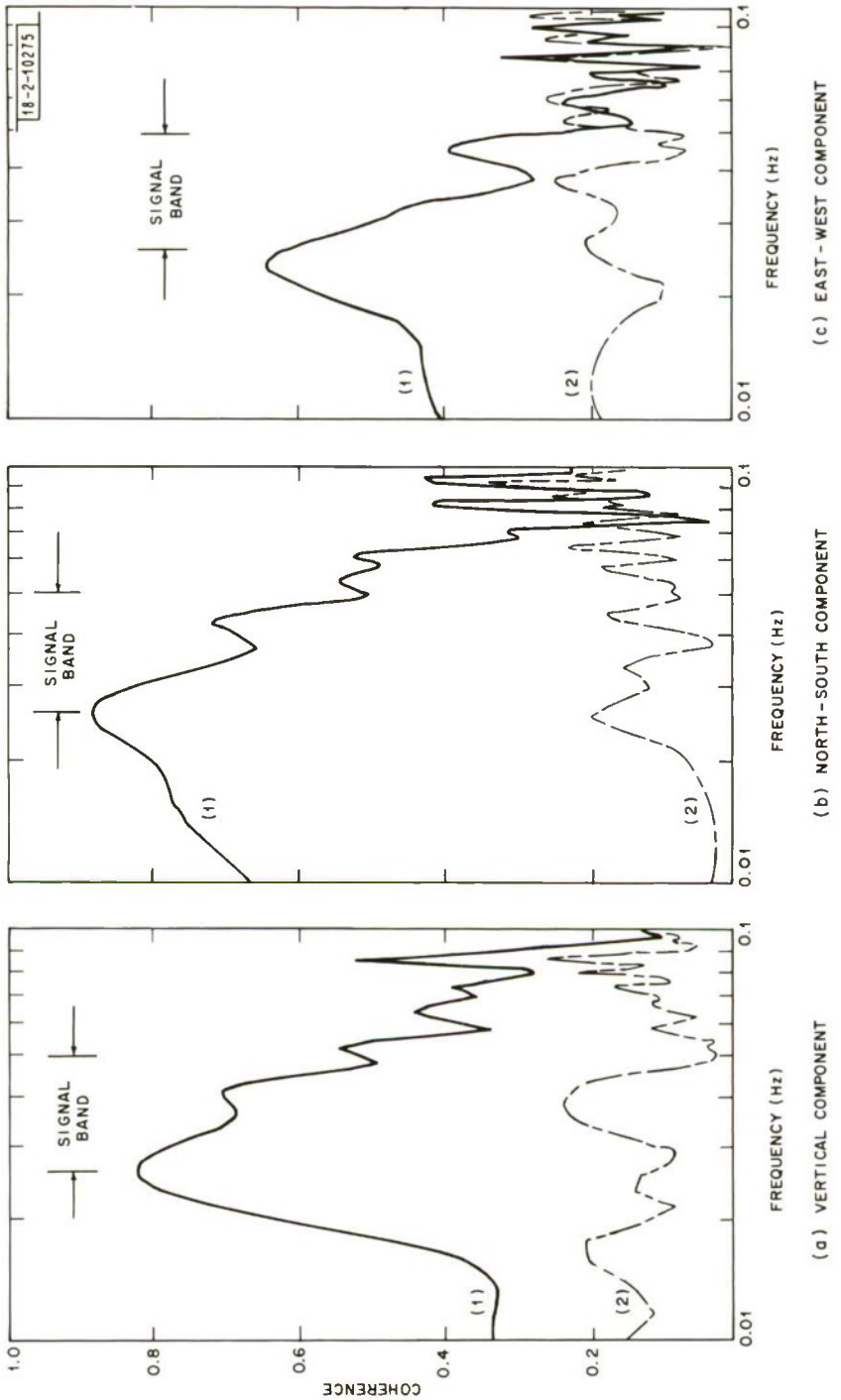

Fig. V-2. From data shown in Fig. V-1 are the computed coherencies between microbarograph and seismometer outputs (1), and microbarograph output and seismometer output with predicted noise subtracted (2) for each component of seismometer (a) vertical, (b) north-south, and (c) east-west.

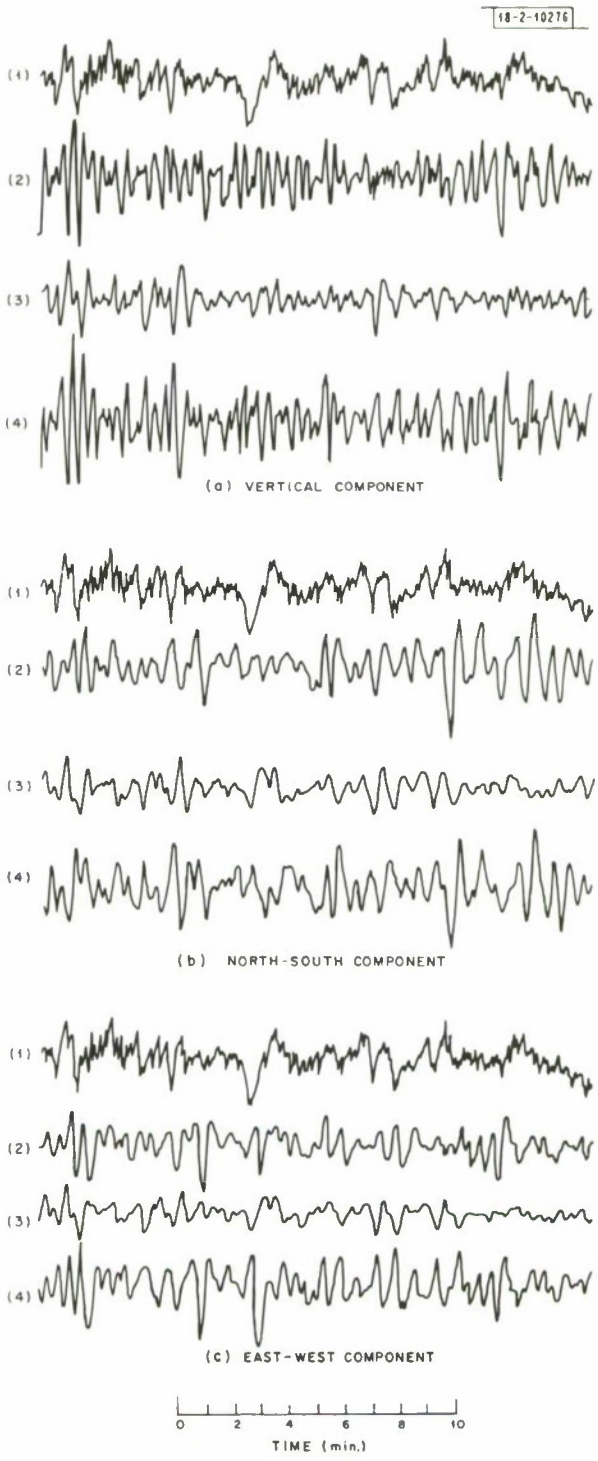

Fig. V-3. Data from LASA site A0 beginning 19h 50m 00s on 1 July 1967. As in Fig. V-1 for each of three components of seismometer (a) vertical, (b) north-south, and (c) east-west are shown seismometer output (2), predicted noise in that output (3), and seismometer output minus predicted noise (4). In each case, (1) is microbarograph output, but predicted noise has been computed from microbarograph output using transfer functions calculated from data of Fig. V-1.

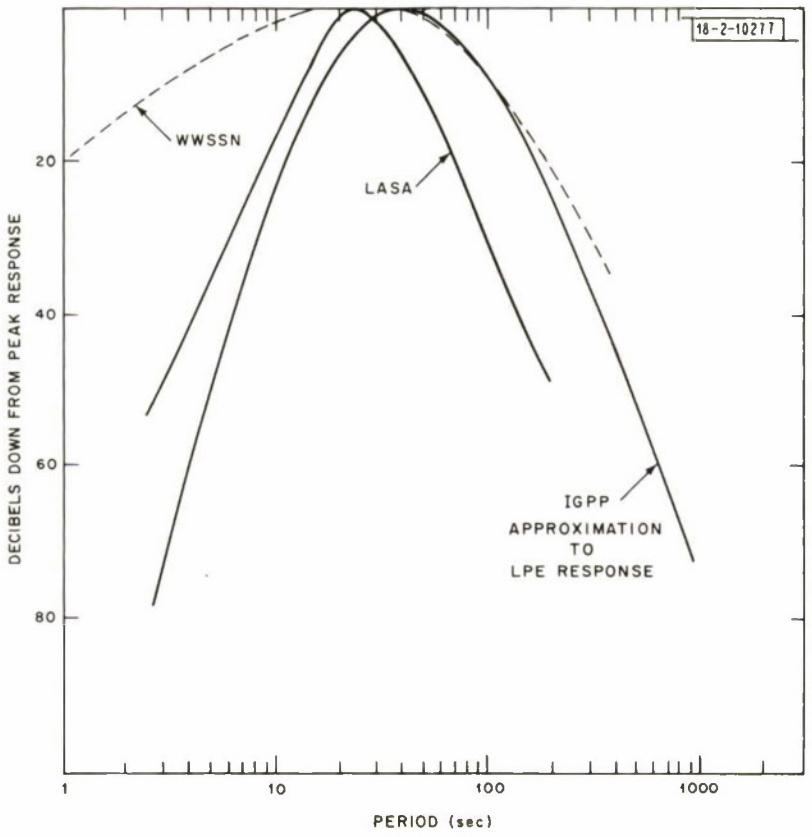

Fig. V-4. Relative response curves of long-period instruments of WWSSN, LASA and IGPP approximation to Lamont LPE.

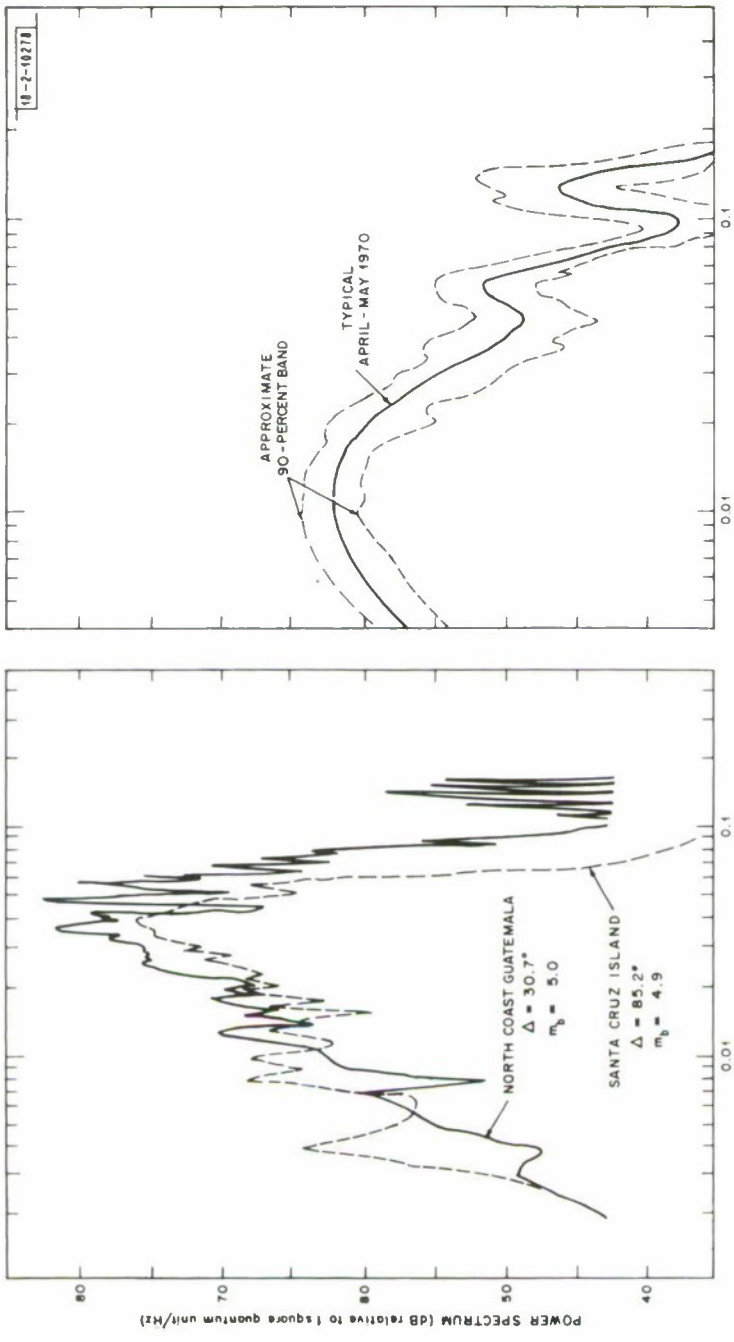

Fig. V-5. Signal and noise spectra measured from IGPP instrument. (a) Two earthquakes; (b) noise samples in April and May 1971.

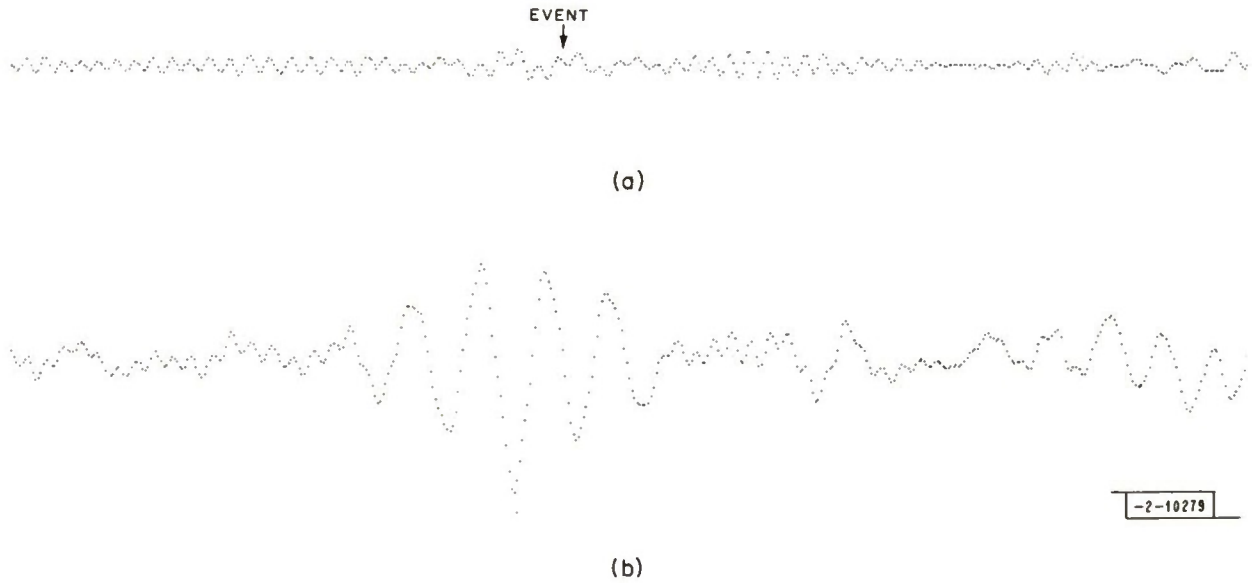

Fig. V-6. (a) Filtered (to give ~0-dB signal-to-noise ratio) and (b) unfiltered IGPP recording of Greek earthquake. Signal reduced about 23 dB by filtering.

VI. DATA-PROCESSING FACILITIES

A. LINCOLN COMPUTER FACILITIES

Floating-point hardware has been ordered for the two PDP-7 computers. When installed, this hardware will speed up by an order of magnitude floating-point operations (now done by software routines using the fixed-point hardware). The Fortran system is being reprogrammed to take advantage of this hardware. The new internal arithmetic library subroutines will operate about 5 times faster, and the science library (sines, exponents, etc.) will operate about 50 times faster. Machine language programs can take full advantage of this hardware and speed up a floating operation by about 10 times over the old Fortran system.

A half-hour 16-mm sound film has been made of the Data Analysis Console demonstrating its various features. This film is available to anyone upon request. A completely revised report on the Analysis Console is also being prepared and will be available to those interested.

P. L. Fleck, Jr.

B. IMPROVED LIBRARY ACCESS

Because of the large numbers both of magnetic tapes (about 10,000) that have been acquired over the last few years, and of epicenters that are reported annually by NOS, SAAC and the International Seismological Center, the process of associating epicenter data with our tape library is being adapted to the Lincoln Information Storage and Associative Retrieval System (LISTAR).† This is an on-line system which will permit the user to define, search, modify and cross-associate data files. In our case, the two data files will contain epicenter data from all sources and magnetic-tape data such as the tape start time, array name and tape location. Input of seismic data into this system will provide a real test as to the usefulness and speed of this particular data retrieval system since our data base will vastly exceed any data base previously used. When the seismic data are finally entered into the system, the user will be able to search the hypocenter file or the tape file on any specific parameter or set of parameters and conditions. For example, a user may wish a list of all tapes that contain earthquakes of magnitude 5.0 or greater, with depths less than 60 km from the Kuril Islands that were recorded on both LASA and NORSAR tapes in our library. It is expected that the LISTAR system will produce this list within 10 or 15 minutes. Such a manual search through all the tape listings and epicenter listings could take several days.

Construction of the epicenter data file is now under way. Initially, the epicenter data file will contain upwards of 100,000 entries obtained from as many reporting agencies as will be convenient. It is anticipated that the annual increase in this file will be about 20,000 entries. A second data file, our tape library file, will initially contain about 8000 entries and be increased by 1500 entries annually.

R. M. Sheppard

---

†"A User's Guide to LISTAR," Lincoln Manual 94, Lincoln Laboratory, M.I.T. (October 1970), DDC AD-714108.

VII. THE INNER CORE

A. DETECTION OF THE PHASE PKJKP

Since its discovery in 1935, the Earth's inner core has been assumed to be a solid, but attempts to detect seismic waves which travel through it as shear waves have always failed. There have been two reasons for this failure: uncertainty of the shear velocity in the inner core and thus of where to look for the seismic waves, and the likelihood that any such waves would be extremely small and might be masked by other, larger phases. Solutions to both problems are now available, however, so a search for the phase PKJKP was undertaken.

In the first place, available free oscillation data, particularly for overtones of the Earth's spheroidal modes, are now able to detect the inner core's rigidity and to make a rough estimate of its value. Thus, it is possible to calculate at which distances and travel times PKJKP should be largest. Secondly, large seismic arrays such as LASA and NORSAR can be used to separate PKJKP from "noise" consisting of phases with different apparent velocities. Normal microseismic noise is of no concern here, because of the size ($m_b \geq 6.0$) of the events used.

Nine large earthquakes of various depths in the distance range from 70° to 125° (out of 38 events examined visually) have been subjected to velocity spectral analysis (Vespa, see Davies, et al.[†]) using data from LASA. Of these, five had phases whose apparent velocities could be determined reliably. The principal source of confusion in this respect comes from sidelobes in the wavenumber response of the array, so care has been taken to reject signals (some probably real) whenever the possibility of such confusion arises.

Figure VII-1 shows the observed travel times and $dT/d\Delta$ values for these phases, as well as two theoretical curves, which suggest that the inner core has a shear velocity of about 2.95 ± 0.1 (which may decrease with depth). A comparison of the waveforms of PKKP and PKJKP consistently indicates that PKJKP is depleted in frequencies above about 0.5 Hz, but that otherwise the signal shapes are remarkably similar. We have obtained a rough estimate of the Q for the J phase of 500 to 1000 by comparing the waveform of PKJKP with that of PKKP after subjecting it to an attenuation filter.[‡]

B. R. Julian
D. Davies
R. M. Sheppard

B. STRUCTURE OF THE INNER-CORE BOUNDARY

A very interesting prospect arises from the work reported in Sec. I by Davies – a means of determining the fine structure of the inner-core boundary. If we take PcP as a source function and deconvolve it from PKiKP, then the resulting time function should be a measure of the reflectivity at the inner-core boundary as a function of depth. The assumption is that the outer core has a very sharp boundary – which seems justifiable from the strong similarity between PcP and PKKKP. Figure VII-2 shows the transfer function for inner-core reflection as a function

† D. Davies, E. J. Kelly and J. R. Filson, "Vespa Process for the Analysis of Seismic Signals," Nature 232, 8-13 (1971).

‡ E. W. Carpenter, "Absorption of Elastic Waves – an Operator for a Constant Q Mechanism," Atomic Weapons Research Establishment Report 0-43/66, Her Majesty's Stationery Office, London (1966).

of time. There is obvious structure over an interval of at least 2 sec, from which we infer that the inner-core boundary is not sharp to better than 10 km. This is an early conclusion and subject to change when more data have been examined. Visual inspection of the signal following PKiKP suggests that there may be structure for a further 100 km into the inner core.

D. Davies
C. W. Frasier

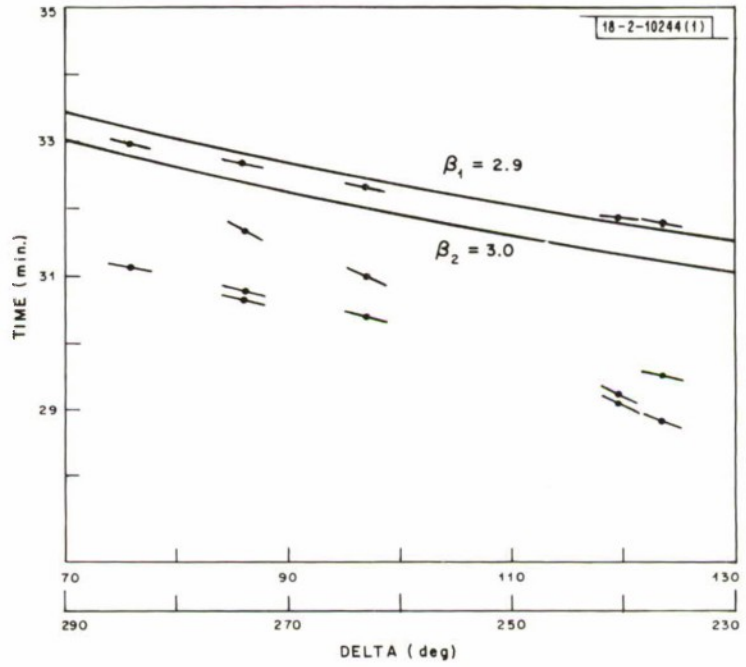

Fig. VII-1. Observed travel times and dT/dΔ values for PKJKP, with theoretical curves for inner-care velocities (assumed constant) of 2.9 and 3.0 km/sec. Data are alsa shawn far variaus branches of phase PKKP.

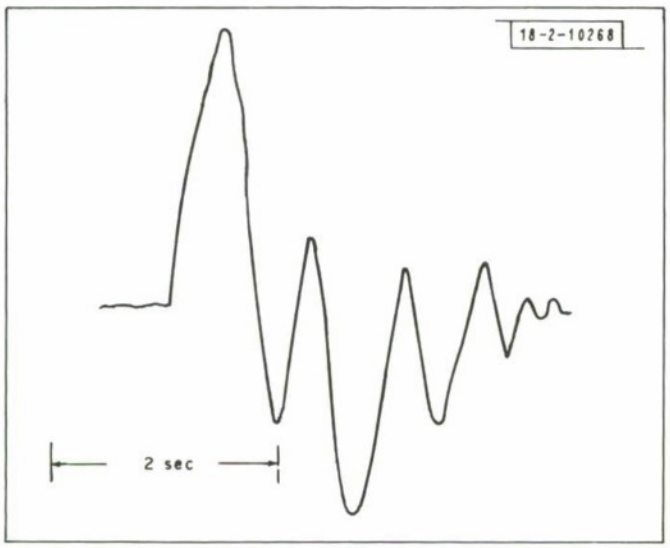

Fig. VII-2. A measure of reflectivity as a function of time at inner-core boundary.

DOCUMENT CONTROL DATA – R&D

(Security classification of title, body of abstract and indexing annotation must be entered when the overall report is classified)

1. ORIGINATING ACTIVITY *(Corporate author)* Lincoln Laboratory, M.I.T.	2a. REPORT SECURITY CLASSIFICATION Unclassified 2b. GROUP None

3. REPORT TITLE

Seismic Discrimination

4. DESCRIPTIVE NOTES *(Type of report and inclusive dates)*

Semiannual Technical Summary Report – 1 July through 31 December 1971

5. AUTHOR(S) *(Last name, first name, initial)*

Davies, David

6. REPORT DATE	7a. TOTAL NO. OF PAGES	7b. NO. OF REFS
31 December 1971	80	36

8a. CONTRACT OR GRANT NO. F19628-70-C-0230 b. PROJECT NO. ARPA Order 512 c. d.	9a. ORIGINATOR'S REPORT NUMBER(S) Semiannual Technical Summary, 31 December 1971 9b. OTHER REPORT NO(S) *(Any other numbers that may be assigned this report)* ESD-TR-71-325

10. AVAILABILITY/LIMITATION NOTICES

Approved for public release; distribution unlimited.

11. SUPPLEMENTARY NOTES	12. SPONSORING MILITARY ACTIVITY
None	Advanced Research Projects Agency, Department of Defense

13. ABSTRACT

New short-period data on source functions both of explosions and earthquakes are reported. Studies of wave propagation in inhomogeneous regions of the earth are described. First results from NORSAR are presented. Long-period noise and signal observations have been made, and some idea of NORSAR's discriminative capability is emerging. Network approaches to discrimination are being expanded. Major improvements in P-wave detection capability are in sight, with joint array and network analysis. New programs are being applied to the rapid acquisition of library information on seismic events. An increasing use of LASA for other geophysics projects is apparent.

14. KEY WORDS

seismic array seismometers seismology

U.S. GOVERNMENT PRINTING OFFICE: 1972–704-102/24